



# 1 Continental-scale prediction of hydrologic signatures and processes

2 Ryoko Araki<sup>1,2</sup>, Anne Holt<sup>1</sup>, John C. Hammond<sup>3</sup>, Admin Husic<sup>4</sup>, Gemma Coxon<sup>5</sup>, Hilary K. McMillan<sup>1</sup>

3 <sup>1</sup>Department of Geography, San Diego State University, San Diego, CA, USA.

4 <sup>2</sup>Department of Geography, University of California, Santa Barbara, Santa Barbara, CA, USA.

5 <sup>3</sup>U.S. Geological Survey, Maryland–Delaware–DC Water Science Center, Baltimore, MD, USA.

6 <sup>4</sup>Department of Civil and Environmental Engineering, Virginia Tech, Blacksburg, VA, USA.

7 <sup>5</sup>School of Geographical Sciences, University of Bristol, Bristol, UK.

8 Correspondence to: Ryoko Araki (rarak159@sdsu.edu; rarak@ucsb.edu) and Hilary McMillan (hmcmillan@sdsu.edu)

9  
10 **Abstract.** Understanding how dominant hydrologic processes and their drivers vary across diverse continental-scale  
11 landscapes is critical for hydrologic modeling and water management applications. Our research addresses this question by  
12 synthesizing large-sample watershed datasets, Caravan and GAGES-II, and developing random forest models to identify  
13 patterns in hydrologic behavior. We assessed dominant processes by examining hydrologic signatures—summary indicators  
14 of watershed behavior derived from hydroclimatic time series and random forest models across 14,146 gauged U.S. watersheds.  
15 The results reveal clear continental-scale gradients in hydrologic processes, including baseflow, overland flow, storage, and  
16 water balance losses. Our map of dominant processes highlights, for example, the transition from baseflow to fast responses  
17 and back to baseflow along the elevation gradient from the Appalachian spine, through the Piedmont, to the Eastern Coastal  
18 Plain; a distinct outer ring around the Great Lakes region; and sharp contrasts between coastal and inland processes in the  
19 West. Variable importance analysis from random forest models show that processes in the western U.S. are primarily controlled  
20 by climate, whereas in the eastern U.S., soil, geology, and topography play larger roles, with distinct human influences apparent  
21 in urban areas. Our estimates of dominant processes and their drivers provide a framework to extend process knowledge from  
22 research watersheds to the continental scale, assess current hydrological understanding, and evaluate hydrological model  
23 structures.

## 24 1 Introduction

### 25 1.1 Identifying hydrologic processes at large scales

26 Estimating the contributions of different hydrologic processes to streamflow generation at a continental scale is essential for  
27 flood forecasting and water resources management. Optimal management strategies, including the design of grey and green  
28 infrastructure, differ depending on which processes dominate hydrological response (Oswald et al., 2023; Thompson et al.,  
29 2020), which vary substantially by regional environmental conditions (Blöschl, 2006; Paola et al., 2006; Penna, 2024).  
30 Understanding how water is partitioned, stored, and transported through different parts of the terrestrial systems is a  
31 fundamental question in the hydrologic sciences (Brooks et al., 2015). To simulate a diverse set of processes at large-scale, a  
32 new generation of hydrologic models with flexible and heterogeneous structures has emerged (Clark et al., 2015; Frame et al.,  
33 2025; Johnson et al., 2023). However, despite these technological advances, we still lack an estimate of dominant hydrologic



34 processes controlling streamflow generation at continental scales (McMillan et al., 2025; Reinecke et al., 2025). Developing  
35 this understanding is a critical step toward unified hydrologic theory (Sivapalan, 2005) and can provide a blueprint for robust  
36 model development and informed decision making.

37

38 Previous efforts to map multiple hydrologic processes at continental scales are scarce. Instead, studies at large scale have  
39 typically focused on one process while others have studied multiple processes for single or small groups of watersheds.  
40 Examples include studies that examined the likelihood of infiltration excess flow occurrence by comparing whether rainfall  
41 intensity exceeds saturated hydraulic conductivity (Buchanan et al., 2018); baseflow indices and their drivers globally (Beck  
42 et al., 2013; Xie et al., 2024); and the strength of runoff-storage connectivity using a correlation between anomalies in  
43 streamflow gauge and satellite water storage observations (Fang and Shen, 2017). A study in Alaska shows that the use of  
44 multiple streamflow statistics can help distinguish and assign hydrologic regions (Barnhart et al., 2022). Model-aided studies  
45 have simulated global patterns of multiple indices: water partitioning into green and blue water, streamflow response elasticity  
46 to rainfall, and streamflow flashiness (Ji et al., 2025), U.S.-wide indices for water balance seasonality (Berghuijs et al., 2014).  
47 Another model-based approach has involved inferring hydrologic processes through parameter sensitivity analysis (Hay et al.,  
48 2023). These synthesis studies present promising descriptions of spatial patterns and directions for future progress toward a  
49 holistic understanding of runoff generation mechanisms, which still remains elusive.

50

51 Much of the research for generalizing watershed behaviors has focused on summarizing flow regimes (Dettinger and Diaz,  
52 2000; Lane et al., 2017; Lee et al., 2015; Lins, 1997) and predicting shifts in flow regime under future climate (Brunner et al.,  
53 2020; Hodgkins et al., 2024). Many studies cluster streamflow gauges using flow indices targeting general (Almagro et al.,  
54 2024; Ariano and Ali, 2025; Mosley, 1981; Wu et al., 2021), intermittent (Sauquet et al., 2021), or seasonal streamflow patterns  
55 (Dhungel et al., 2016; Haines et al., 1988; Kennard et al., 2010). However, most of these studies aim to define the similarity  
56 of flow regimes rather than the underlying runoff generation processes. Furthermore, the results from clustering approaches  
57 are constrained to gauged locations and lack spatial coherence, making it challenging to extrapolate to ungauged watersheds.

58

59 To estimate watershed processes in ungauged locations, hydrologists have conventionally used maps derived from  
60 physiographic datasets. For example, in the United States context, the Environmental Protection Agency's Ecoregions  
61 (Omernik, 1987, 2004), an ecosystem classification based on the physical and biotic characteristics, is a common reference  
62 when discussing hydrologic processes (Falcone et al., 2010). Other classifications include the United States Geological  
63 Survey's Water Resources Regions (Seaber et al., 1987) based on streamflow networks, Hydrologic Landscape Regions  
64 (Santhi et al., 2008; Winter, 2001; Wolock, 2003a) based on physiographic and climatic datasets, and the United States  
65 Department of Agriculture's Hydrologic Soil Groups (Web Soil Survey, 2025) based on soil surveys. Nevertheless,  
66 regionalization based on physiographic data often fails to capture the full variability of watershed behavior (Ali et al., 2012;  
67 Oudin et al., 2008) because hydrologic processes can differ even among physiographically similar watersheds (McMillan et



68 al., 2014). Capturing watershed processes at a continental scale calls for a scalable method to draw information from  
69 hydroclimatic datasets. To date, no studies have attempted to develop comprehensive maps of runoff generation processes  
70 based on streamflow observations that can effectively capture watersheds' functions.

## 71 **1.2 Hydrologic signatures links to processes**

72 Hydrologic signatures are metrics that quantify hydrologically-relevant dynamics, and offer a promising way to infer watershed  
73 processes with minimal data requirements (McMillan, 2021). Hydrologic signature calculations require only widely-available  
74 datasets, such as streamflow and precipitation, and can be related to various watershed processes, such as runoff generation  
75 and water storage dynamics (McMillan, 2020; Wlostowski et al., 2021). Using hydrologic signatures, expert knowledge, and  
76 landscape characteristics, Fenicia and McDonnell (2022) inferred dominant runoff processes and developed perceptual models  
77 at the regional scale; and Pechlivanidis and Arheimer (2015) mapped process differences at the national scale in India.  
78 Hydrologic signatures can capture the functional streamflow responses to climatic forcings and can discriminate different  
79 processes across landscapes (Araki et al., 2022; Gnann et al., 2020, 2021a; Janssen and Ameli, 2021). This enables a signature-  
80 based exploration of the relationship between landscape form and function (Bracken et al., 2013; Sivapalan, 2005).

## 81 **1.3 Predicting hydrologic signatures using watershed attributes**

82 Watershed attributes describe the physical characteristics of watersheds, which can be used to identify the drivers of hydrologic  
83 processes and to transfer hydrological knowledge to ungauged locations (Tarasova et al., 2023). The link between watershed  
84 attributes and signatures of streamflow response can be explored via machine learning approaches on large watershed samples.  
85 Regional and global applications include studies in the U.S. (Addor et al., 2018; Janssen and Ameli, 2021; Wu et al., 2021),  
86 Australia (Trancoso et al., 2017), Zimbabwe (Mazvimavi et al., 2005), Brazil (Almagro et al., 2024), Europe (Kuentz et al.,  
87 2017), and globally (Beck et al., 2015). Across all studies, climate emerged as the primary control on signatures. Non-climatic  
88 factors (i.e., landscape attributes), such as soil, geology, vegetation cover, and topography, had weak or limited predictive  
89 power. However, substantial evidence from field-based studies shows that landscape forms are a primary control of watershed  
90 function (Angermann et al., 2017; Fan et al., 2019; Jackisch et al., 2017; Jefferson et al., 2010; Lohse and Dietrich, 2005;  
91 Pfister et al., 2017; Zimmer and Gannon, 2018).

92  
93 Weak predictive power of non-climatic drivers can be attributed to lack of high-resolution, accurate landscape attributes that  
94 describe regionally important processes (Gnann et al., 2021a; Tarasova et al., 2023). For example, wetlands are key regulators  
95 of low flows in the U.S. (Worland et al., 2018) and have been left out of previous studies (Addor et al., 2018). Similarly,  
96 weathering and glaciation have primary impacts on baseflow storage and generation (Neff et al., 2005; Tague and Grant, 2004),  
97 but rock permeability and porosity predictors did not clearly capture the relationship (Wu et al., 2021). Coarse spatial resolution,  
98 or limited quality and consistency of global datasets may reduce their predictive power (Beck et al., 2015; Tarasova et al.,  
99 2023). Regional analysis can mitigate climate influence and elucidate the contribution of non-climatic drivers, such as regional



100 random forest models that revealed physiographic and anthropogenic controls on flow regimes (Almagro et al., 2024;  
101 Hammond et al., 2021). However, smaller regional sample sizes may limit prediction accuracy if datasets only provide tens of  
102 watersheds per region (Willard et al., 2024).

103

104 Lastly, the quality of signatures can compromise data-driven model performance and interpretation for process understanding.  
105 Examples include the sensitivity of flow duration curve slope to measurement errors (McMillan et al., 2017), the sensitivity of  
106 signatures to rating curve uncertainties (Westerberg et al., 2016), lack of process representativeness (McMillan et al., 2022),  
107 and inaccurate parameterization of storm separation algorithms (McMillan et al., 2023). Minimizing the impact of signature  
108 uncertainty is important for differentiating different regional watershed functionalities (Westerberg et al., 2016).

109

#### 1.4 Aims of the paper

110

This study presents the first hydrologic processes map for the contiguous United States (CONUS). We synthesized hydrologic  
111 signatures as process indicators, going beyond pattern identification from single signatures. We hypothesize that signature  
112 combinations can represent six key hydrologic processes (McMillan, 2020; McMillan et al., 2022): baseflow and storage,  
113 water balance and seasonal flow variability, and saturation and infiltration excess overland flow. Using random forest models,  
114 we demonstrate the explanatory power of landscape metrics to predict hydrologic signatures and their regional variations, and  
115 thus the underlying processes, across CONUS.

116

117

We address the limitations of previous studies in predicting hydrologic signatures. First, we improved the quality of non-  
118 climatic attributes by: (i) incorporating new geological and wetland landscape attributes that have demonstrated strong  
119 connections to baseflow processes (Holt and McMillan, 2025); and (ii) utilizing watershed attributes from GAGES-II datasets  
120 (Falcone, 2011), derived from survey-based and higher-resolution products. Second, we interpret random forests using Shapley  
121 values (Shapley, 1953) following Husic et al. (2025), as well as permutation importance values within a regional model-  
122 building approach, following Hammond et al. (2021), which extends prior work to elucidate the regional contributions of non-  
123 climatic, landscape attributes to hydrologic processes. Furthermore, our work assessed 14,146 U.S. watersheds and was trained  
124 on 10,261 watersheds, nearly ten times more sample watersheds than previous studies; we leverage the Caravan and GAGES-  
125 II—the most extensive open-source large-sample datasets currently available (Falcone, 2011; Kratzert et al., 2023). Third, we  
126 utilize a set of hydrologic signatures proven robust across large-sample watershed studies and have a clear connection to  
127 critical-zone processes (McMillan et al., 2022), with their parameters further tuned to local storm characteristics. With these  
128 improvements, we expand watershed coverage and uncover more detailed spatial patterns of watershed processes than  
129 previously possible, using widely-available hydroclimatic datasets and physiographic attributes.



130 **2 Data**

131 We used two primary sources of streamgages and watershed attribute data to expand the number of samples: Caravan v1.5  
132 (Kratzert et al., 2023, 2024) and U.S. Geological Survey GAGES-II (Falcone, 2011; Falcone et al., 2010). See Fig. 1 for the  
133 spatial distribution of the study watersheds. Caravan is an open-source dataset of global watersheds; its CONUS subset consists  
134 of 9,234 watersheds sourced from CAMELS-US (Addor et al., 2017) and HYSETS (Arsenault et al., 2020). GAGES-II is a  
135 geospatial dataset of 9,067 watersheds in the United States, selected for their quality to characterize natural and altered flow  
136 regimes.

137 **2.1 Hydroclimatic dataset**

138 We calculated hydrologic signatures listed in Table 1 using daily hydroclimatic timeseries data from watersheds within the  
139 contiguous United States (CONUS). For Caravan watersheds, we used U.S. Geological Survey (USGS) streamflow  
140 measurements paired with daily ERA5-Land forcings provided. For the GAGES-II watersheds, we obtained the USGS  
141 streamflow records (U.S. Geological Survey, 2025) using the dataRetrieval package (DeCicco et al., 2018) and gridMET  
142 forcings from Wieczorek et al. (2023). For calculating infiltration excess overland flow signatures of Wu et al. (2021;  
143 “*RC\_Pint*”), we used the hourly precipitation from the North American Land Data Assimilation System 2 (NLDAS-2; Xia et  
144 al., 2012) provided through CAMELSh: a Large-Sample Hourly Hydrometeorological Dataset and Attributes at Watershed-  
145 Scale for CONUS (Tran, 2025; Tran et al., 2025).

146 **2.2 Watershed attributes**

147 We combined watershed attributes from three sources: (1) Caravan, (2) GAGES-II, and (3) geologic age and wetland attributes  
148 (Holt and McMillan, 2025). We added average geologic age and isolated wetland fraction metrics because of their strong link  
149 to baseflow processes, which were missing from previous large-sample analyses (Holt and McMillan, 2025). From the Caravan  
150 and Holt & McMillan (2025) attribute sets, we excluded binary or categorical attributes, monthly climate variables,  
151 uninformative attributes for the CONUS context (e.g., permafrost extent, gross domestic product), and highly correlated  
152 attributes (Spearman's rho > 0.8 or < -0.8; see Text S1). Where available, Caravan attributes were substituted with GAGES-II  
153 attributes, as described in Section 3.2 and Table S1. Table 2 lists the 23 attributes used in the random forest analysis.

154 **3 Method**

155 **3.1 Calculating hydrologic signatures**

156 A total of 12 signatures (four baseflow and groundwater signatures, four water balance and seasonality-related signatures, and  
157 four overland flow signatures) were used to characterize hydrologic dynamics (see Table 1). The signatures were selected



158 based on their reliability in representing processes (McMillan et al., 2022). We calculated signatures using the TOSSH toolbox  
159 (Gnann et al., 2021b) and tuned the parameters for event separation for each hydroclimatic region (see Tables S2, S3).

160 **3.2 Training random forest models and predicting hydrologic signatures**

161 We developed random forest models to examine potential drivers of hydrologic processes. Random forest models have been  
162 widely used for this task (Eng and Wolock, 2022; Lapides et al., 2023; Zipper et al., 2021) for their interpretability, relatively  
163 low computational demands, and robustness to multi-collinearity (Addor et al., 2018). For each signature, we constructed a  
164 random forest model to predict its values based on watershed attributes using the caret R package (Kuhn, 2008; R Core Team,  
165 2024). Each model used 500 trees with the optimal number of features randomly resampled at each split, selected by  
166 minimizing root mean squared error (RMSE) through 10-fold cross-validation.

167

168 Only quality-controlled observations were used for training. Training on all Caravan watersheds yielded  $R^2 < 0.4$  for many of  
169 the signatures, so we limited the training samples to the 4,748 Caravan watersheds with streamflow gauge IDs overlapping  
170 with GAGES-II to attain model performance comparable to previous studies (see Text S2). Furthermore, we omitted  
171 watersheds from our training sample with short or incomplete streamflow records or uncertain watershed boundaries. First, we  
172 excluded watersheds with less than 5 years of streamflow observation record, and those with over 30% missing daily data over  
173 the period where streamflow was recorded. Second, we removed watersheds from our analysis with uncertain topographic  
174 boundaries, showing high discrepancies (>25%) in the estimated drainage area between GAGES-II and Caravan datasets. Third,  
175 for overland flow signature analysis, we excluded snow-dominated watersheds (>20% snow fraction of total precipitation);  
176 this is because our overland flow signatures can be heavily influenced by periods with no flow response due to snow or frozen  
177 conditions. When a gauged watershed was present in both datasets, we prioritized CAMELS over HYSETS, and Caravan over  
178 GAGES-II. This is to ensure the broader applicability of our method across different countries, as Caravan is available at global  
179 scale. This yielded a total 14,403 watersheds for signature analysis (overview in Table S1).

180

181 We then used the trained model to predict hydrologic signatures for 3,885 watersheds where observations did not meet data  
182 quality standards. Preliminary experiments showed improved model performance when the watershed attributes were derived  
183 from higher-resolution datasets based on detailed field surveys, such as in GAGES-II and (Holt and McMillan, 2025).  
184 Therefore, we used GAGES-II attributes and when unavailable, used the coarser resolution Caravan attributes (see Table S1).

185 **3.3 Interpretation of hydrologic signatures as process descriptors**

186 We combined signatures calculated from observed streamflow data and predicted with random forest models to develop a  
187 comprehensive map of processes for watersheds across the U.S. (Fig. 1). A bivariate space of hydrologic signatures was used  
188 to infer process dominance. For each selected process, we used the two signatures most strongly related to the process inferred  
189 from previous work (Bolotin and McMillan, 2024; McMillan, 2020; McMillan et al., 2022; Wu et al., 2021). Each signature



190 was categorized based on the quantiles of signatures, from low (0-25%), mid-low (25-50%), mid-high (50-75%), to high (75-  
191 100%). When both of the two target signatures had mid-high (50-75%) or high (75-100%) values, we interpreted this as  
192 indicative of process dominance. This bivariate matrix can highlight the complexity of hydrologic processes where two  
193 signatures do not necessarily show the same trends.

194  
195 The major process hypotheses are as follows (detailed in Table 1): regions with strong baseflow processes would show high  
196 baseflow magnitude (larger *BFI*) and slow baseflow recession (smaller *recession K*); regions with large storage capacity and  
197 retention would show high storage magnitude (larger *AverageStorage*) and more nonlinear recessions (larger *Recession*  
198 *parameter b*); regions with large water balance losses would show smaller runoff ratios (smaller *TotalRR* and *EventRR*);  
199 regions strongly influenced by seasonality in processes (e.g., evapotranspiration, snow) would show variability in the flow  
200 timeseries and recessions (large *Recession a seasonality* and large *variability index*); regions with strong overland flow or  
201 stormflow processes would exhibit strong threshold responses to precipitation (large *threshold value* and high significance,  
202 small *p*-values); regions dominated by infiltration-excess overland flow would show stronger correlation between flow and  
203 precipitation intensity (*RC\_Pint* > *RC\_Pvol*) while regions dominated by saturation-excess overland flow would show stronger  
204 correlation between flow and precipitation volume (*RC\_Pvol* > *RC\_Pint*).

### 205 **3.4 Interpretation of process drivers using Shapley values**

206 We quantified feature importance using Shapley values (Shapley, 1953), which provide a robust and consistent measure to  
207 interpret random forest models (Lundberg et al., 2018). Shapley values represent the average marginal contribution of a feature  
208 (i.e., a landscape attribute) to a prediction, given the effects from all combinations of the considered features. Shapley values  
209 allow for local and global interpretation of machine learning model predictions, helping to uncover site-specific and  
210 generalizable linkages between hydrology and landscape features (Husic et al., 2025). We used the interpretable machine  
211 learning (iml) R package (Molnar et al., 2018) to calculate Shapley values over the training data.

212  
213 To evaluate the regional effects of watershed attributes, we computed summary statistics on Shapley values. Shapley values  
214 are site-specific:  $\phi_x^{(y,i)}$  is the Shapley value calculated for an attribute  $x$  for a signature  $y$  at location  $i$ . Summing the Shapley  
215 values across watershed attributes  $x$  at a single location gives the deviation of the predicted signature value  $y_i$  at location  $i$  from  
216 the mean signature value across all sites. To compare effects of a landscape attribute  $x$  across sites, we normalize Shapley  
217 values by the total absolute contribution from all attributes at a site  $i$ ; this gives a metric for the relative contribution of an  
218 attribute  $x$  to signature  $y$  at site  $i$  as:

$$219 R_x^{(y,i)} = |\phi_x^{(y,i)}| / \sum_{x \in A} |\phi_x^{(y,i)}|$$



220 where  $A$  is the set of all watershed attributes, and  $|\cdot|$  denotes the absolute value. To investigate which types of landscape  
221 characteristics are influential, we classified the watershed attributes into five categories (see Table 2), namely, topography,  
222 land-cover, soil & geology, human alteration, and climate.

223

224 Then, the average relative contribution of category  $k$  for signature  $y$  at location  $i$ ,  $\bar{R}_k^{(y,i)}$ , is calculated as:

225

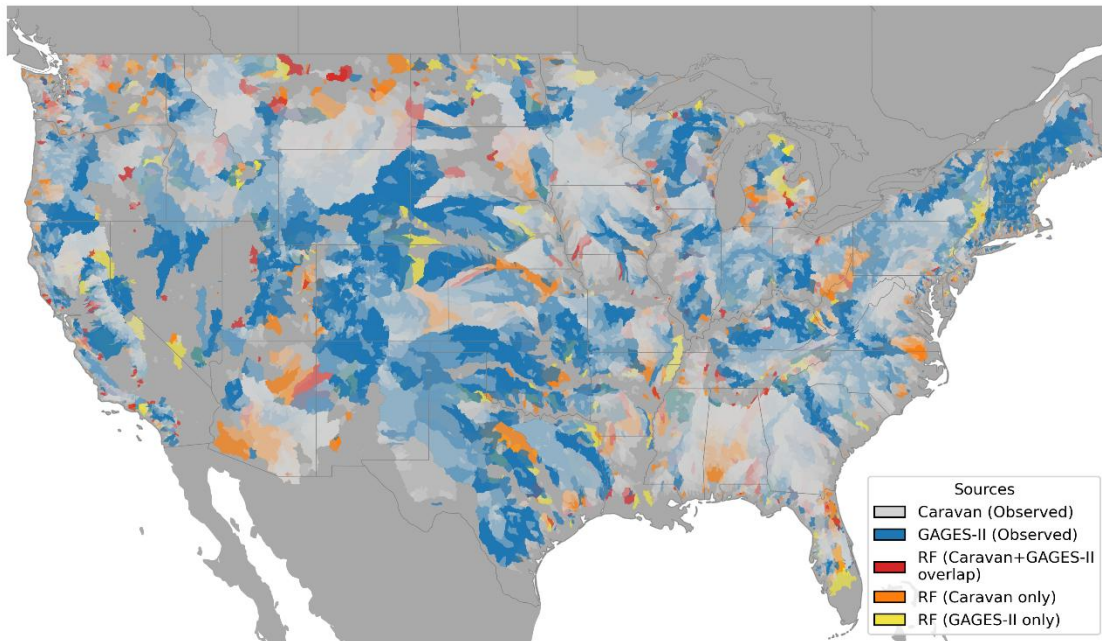
$$\bar{R}_k^{(y,i)} = \frac{1}{K} \sum_{x \in C_k} R_x^{(y,i)}$$

226 , where  $C_k$  is the set of watershed attributes belonging to category  $k$ , and  $K$  is the number of categories (in our case, five).

### 227 **3.5 Interpretation of process drivers using permutation importance**

228 To further evaluate locally important watershed attributes, we computed permutation importance, which measures the change  
229 in model performance when a feature (i.e., a landscape attribute) is removed. Prior work has shown that permutation  
230 importance derived from random forest models trained on regional samples is more effective than a continental approach for  
231 identifying physiographic, landscape controls on hydrologic responses, as it allows assessment under consistent climate  
232 conditions (Almagro et al., 2024; Hammond et al., 2021; Holt and McMillan, 2025). Therefore, we calculated permutation  
233 importance as the average changes in mean squared error (MSE), normalized by its standard deviation using the caret R  
234 package (Kuhn, 2008), from random forest models trained on regional watershed samples. Six climate regions were defined  
235 using a Gaussian mixture model in Scikit-learn (Pedregosa et al., 2011) based on relevant Caravan, GAGES-II, and Hammond  
236 et al. (2023) climate attributes (Table S4), and separate random forest models were trained for each region. Fig. S1 shows the  
237 identified climate regions.

238



239

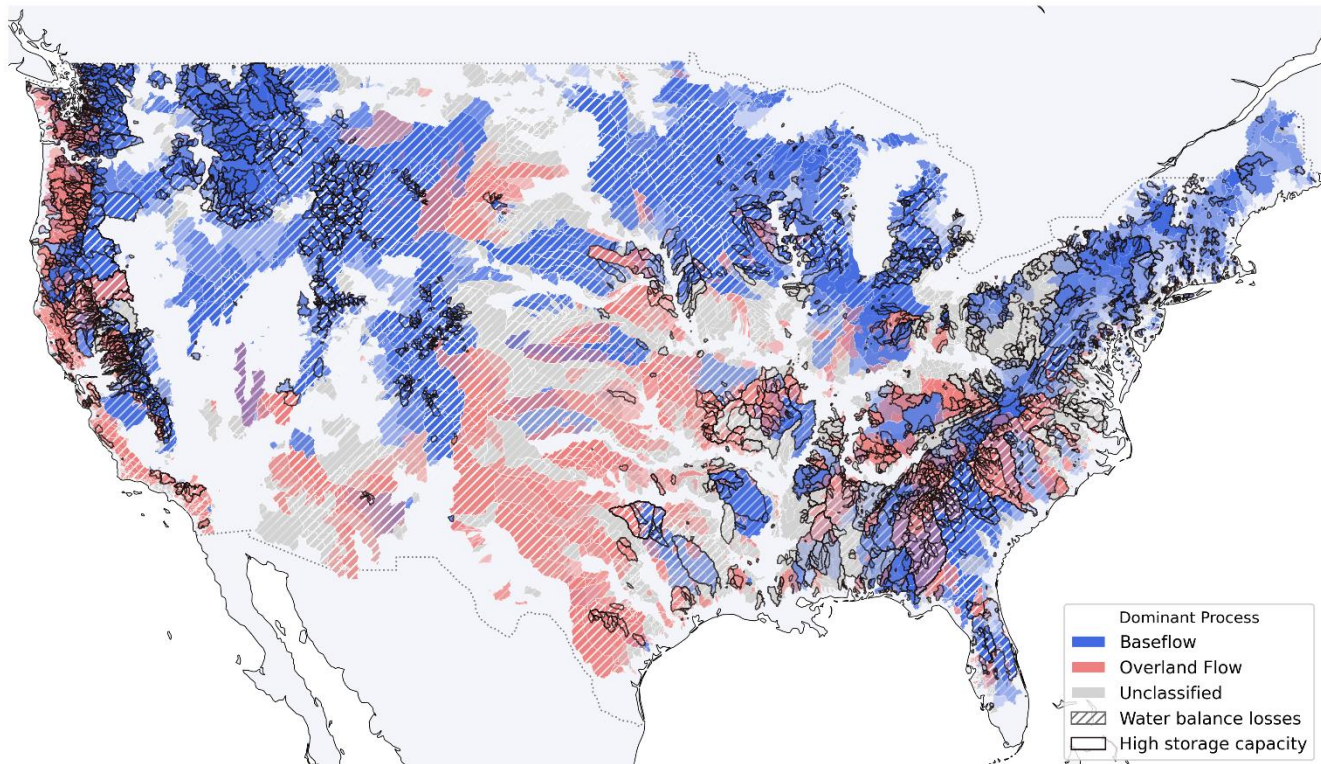
240 **Figure 1: Method used to obtain hydrologic signatures. Signatures are derived either from observed data (“Observed”: Caravan**  
241 **samples, n=7,465; GAGES-II samples, n=2,807; total n=10,261) or predicted using random forest models (“RF”; n=3,885). Predicted**  
242 **samples are categorized as: “Caravan+GAGES-II overlap” (present in both the Caravan and GAGES-II datasets; n=618), “Caravan**  
243 **only” (exclusive to Caravan; n=2,424), and “GAGES-II only” (exclusive to GAGES-II; n=843). State boundaries are indicated by**  
244 **grey lines.**

245 **4 Results**

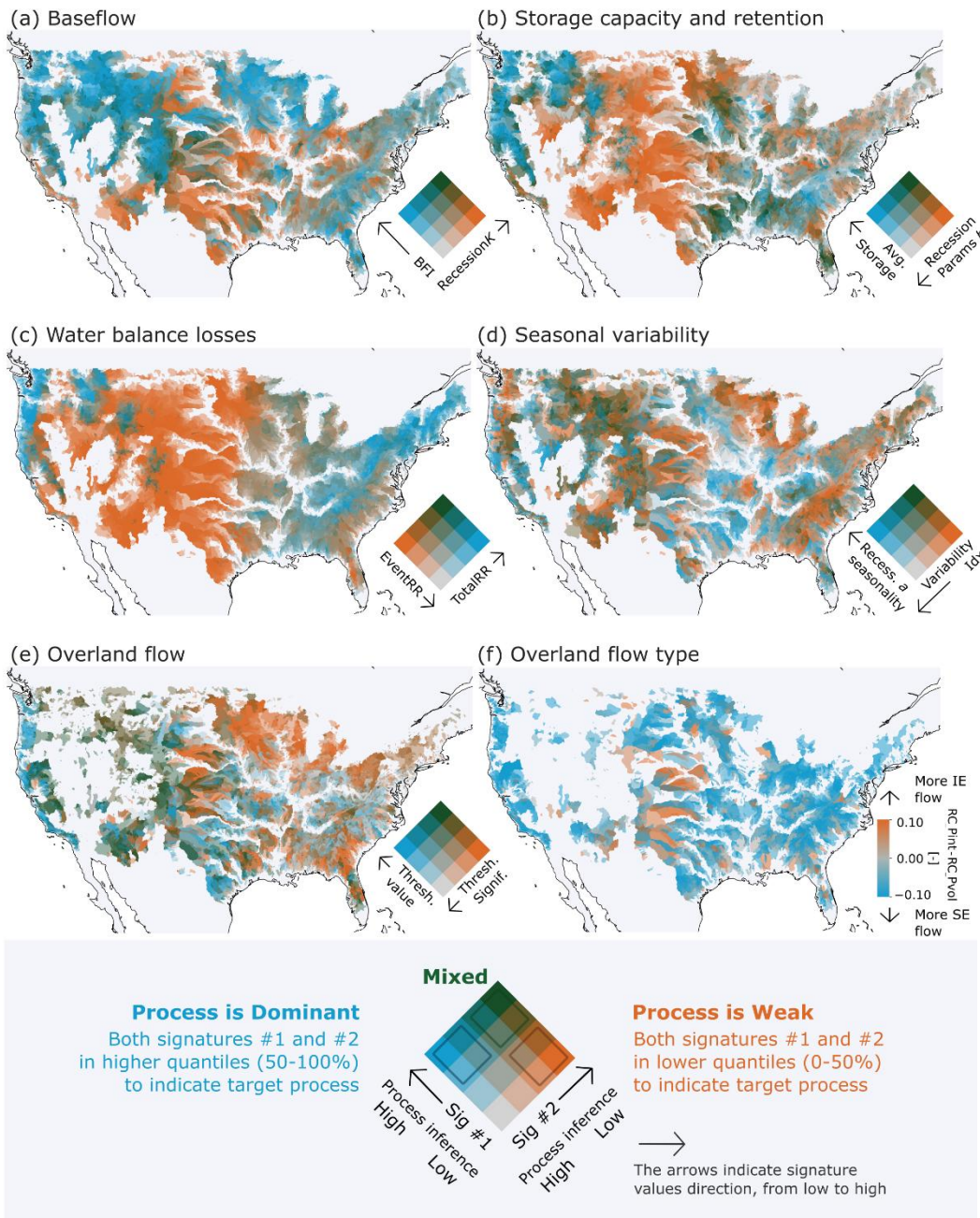
246 **4.1 Mapping dominant processes across the contiguous U.S.**

247 Figures 2 and 3 show the maps of dominant processes derived from the hypotheses outlined in Table 1. Figure 2 presents the  
248 signature of each process hypothesis in a bivariate map. Figure 3 provides a summary, displaying only the selected process  
249 hypothesis when it is deemed dominant (i.e. both signatures are in the mid-high (50-75 %) or high (75-100 %) quantiles).  
250 Together, these maps highlight distinct regional patterns in hydrologic processes across the study area. The following sections  
251 examine these patterns in greater detail by region: the East and South. (Section 4.2.1.), the Midwest and Central (Section 4.2.2.),  
252 and the West and Southwest (Section 4.2.3.).

253

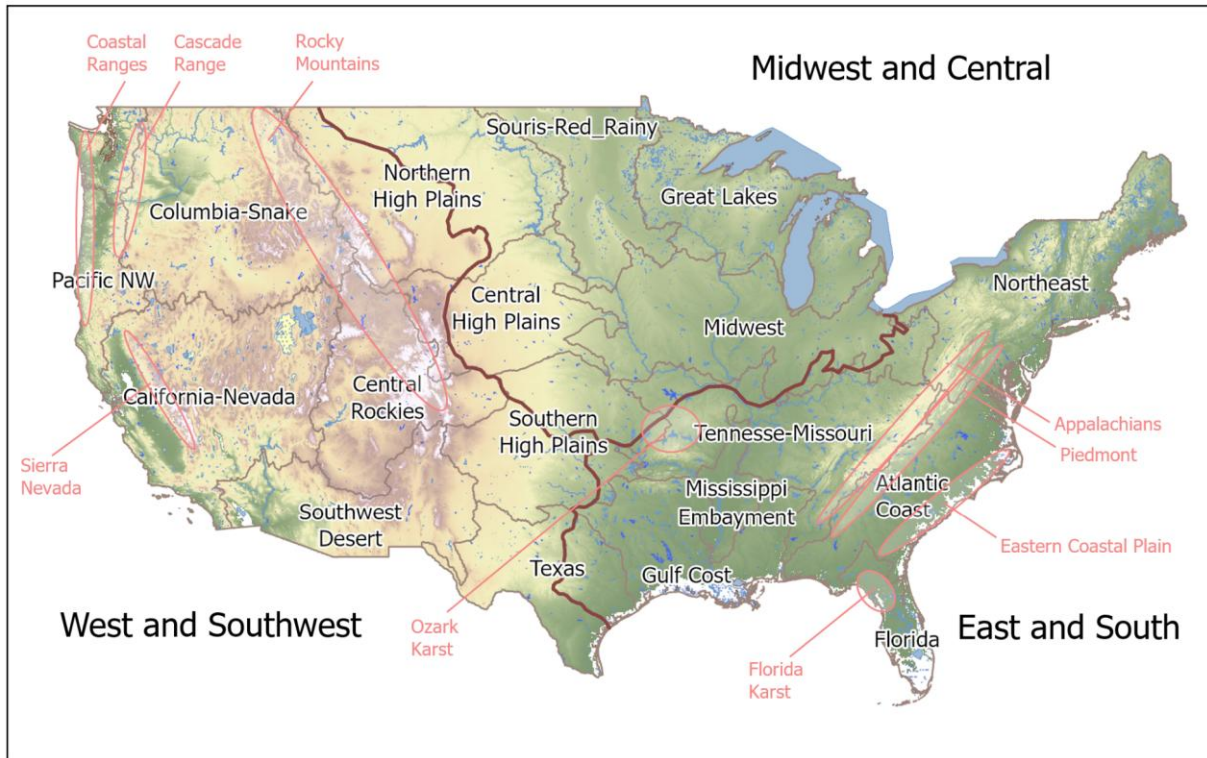


254  
255 **Figure 2: Map of dominant processes estimated based on our hypothesis (defined in Table 1 and Section 3.3). Note that when**  
256 **baseflow and overland flow both occur, their colors are overlaid to give purple hues.**



257

258 **Figure 3:** Hydrologic signatures of each process hypothesis, shown in bivariate maps (a–e). See the legend at the bottom for  
 259 explanation. The high-process quantile from (a) is used to infer “Baseflow” in Figure 2; from (b) to infer “High storage capacity”;  
 260 from (c) to infer “Water balance losses”; and from (e) to infer “Overland flow.” Panel (f) shows the differences between the two  
 261 signatures related to infiltration-excess (IE) flow and saturation-excess (SE) flow (i.e., values of  $RC\_Pint$  minus  $PC\_Pvol$ ). In the  
 262 overland flow panels (e) and (f), watersheds dominated by snow (i.e., where more than 20% of annual total precipitation falls as  
 263 snow) are not shown. For the overland flow type pane (f), watersheds are not shown when the correlations between the event runoff  
 264 coefficient and both rainfall characteristics (i.e., storm rainfall volume and maximum intensity) are negative. For maps of each  
 265 signature value, see Figures S2 and S3.



266

267 **Figure 4: Map of the contiguous United States showing (i) areas described in Section 4.2.1-4.2.3 (East and South, Midwest and**  
268 **Central, West and Southwest; bolded brown line) (ii) geographical boundaries used for the USGS National Water Availability**  
269 **Assessment (Qi and Mason, 2023; Stets et al., 2025; Van Metre et al., 2020) (beige line) (iii) topographic and geological features**  
270 **named in the text (pink annotations).**

271 **4.2 Spatial patterns of hydrologic processes inferred from signatures**

272 **4.2.1 Region 1: East and South**

273 This section describes the East and South of the U.S. (Fig. 4). This humid region has moderate to high precipitation (1,000-  
274 1,500 mm/yr; calculated based on the 10th and 90th percentiles of sample watershed attributes), with low precipitation  
275 seasonality except in Florida. Temperatures vary widely from snow-dominated areas in the NorthEast to subtropical areas in  
276 Florida, with mean annual temperature ranging from 7-19°C (Fig. S4). The landscape is old with deeply weathered soils and  
277 characterized by predominantly low-lying elevation (mean watershed elevation ranges between 40-600m), though there is a  
278 primary elevation gradient from the Appalachian Mountains and Piedmont to the Eastern coastal plains, with peaks exceeding  
279 1,000m (Fig. S8). In Figure 3, signature values show that these climate and landscape conditions produce slowly-varying,  
280 baseflow-dominated flow regimes and mid-quantile signature values showing a lack of hydrologic extremes. Runoff ratios  
281 (*TotalRR* and *EventRR*; Fig. 3c) are moderate or high and seasonal variability in flow and recessions is moderate to low.



282 Storage capacity (*Avg. Storage*) is overall moderate, but recession shapes (*Recession Params b*) are variable (Fig. 3b). Evidence  
283 for overland flow is weak with saturation excess prevailing when it occurs (Fig. 3e,f).

284

285 The gradient along the geographical transect from the Appalachian spine to the Eastern coastal plain is apparent in several  
286 processes. The Appalachians have strong baseflow influence, shown by high baseflow index and slow recessions (Fig. 3a).  
287 Nonlinear recessions (high *Recession Parameter b*; Fig. 3b) indicate multiple groundwater reservoirs supplying baseflow. In  
288 contrast, the Piedmont has lower baseflows and fast recessions, relating to lower storage, a greater fraction of developed land,  
289 and wide, wet valley bottoms that generate a fast response (Zimmer and Gannon, 2018). The Eastern coastal plain, especially  
290 towards the South, has high baseflow and moderate to slow recessions (Fig. 3a). Linear recessions suggest a single dominant  
291 groundwater reservoir supplying baseflow (Fig. 3b). These characteristics reflect the sandy soils, seasonal flooding and  
292 presence of wetlands atop the coastal plain aquifer (Holt and McMillan, 2025; Hupp, 2000). Lower runoff ratios in the coastal  
293 plains indicate losses to deep groundwater including offshore discharge, especially in Florida's karst area (Fig. 3c, S6). The  
294 karst area stands out for its high dynamic storage and seasonality in recessions. Saturation excess dominates overland flow in  
295 the Coastal plain (Fig. 3f), although evidence for overland flow is weak (Fig. 3e) in contrast to a previous study (Wieczorek  
296 and LaMotte, 2010) that suggests the Florida panhandle has the highest fraction of saturation excess overland flow in the US.  
297

298

299 In inland areas such as the valleys of the Tennessee-Missouri region, baseflow is moderate and recessions are relatively fast  
300 (Fig. 3a). The Gulf Coast region has lower baseflow and faster, linear recessions. Although depth to bedrock is high (Fig. S5),  
301 and these areas overlie semi-consolidated sand aquifers, soils are clay-rich and capable of generating infiltration excess flow  
302 (Miller, 1999; Fig. S6). Infiltration excess flow largely occurs in the narrow ocean margin of the Gulf coast region but does  
303 not extend far inland (Fig. 3f). Exceptions to the area's fast runoff occur in the Ozark Mountains and the west of the Mississippi  
embayment where limited areas of high baseflow and slow recessions occur.

304

#### 4.2.2 Region 2: MidWest and Central

305

306 The landscape of the Midwest and Central region is dominated by the gradient from recently-glaciated, sandy, forested  
307 watersheds of the Great Lakes region, to the poorly-drained, clay-rich but highly developed for agriculture and populated  
308 region of the Souris-Red-Rainy and Midwest regions. Across the Midwest and Central area, mean watershed elevation ranges  
309 from 200 to 700 meters, and mean annual precipitation varies from 500 to 1,000 mm. Moving west into the Central and  
310 Northern High Plain regions, elevation gradually increases, precipitation decreases, and population density decreases (Fig. S8,  
311 S4, S7). The region experiences mean annual temperatures between 6 to 13°C. The absence of major topographic barriers  
312 results in a continental climate characterized by intense thunderstorms in summer and heavy snowfall in winter.

313

314 Signature values show that storage capacity is moderate throughout the Midwest (Fig. 3b). Storage in this region is provided  
by a moderate snowpack and high depth to bedrock (Fig. S5). Most of the region was previously glaciated, leaving a thick



315 layer of glacial drift. The soil texture is graded from coarse and sandy around the Great Lakes to clay-rich further South and  
316 West, forming a distinctive outer ring around the Great Lakes region (Miller and White, 1998; Fig. S6). Following this gradient,  
317 there is very low evidence for overland flow around the Great Lakes, changing to stronger evidence further South-West (Fig.  
318 3e,f). Some occurrence of infiltration excess is consistent with evidence of this process from Midwest agricultural watersheds  
319 (Abban et al., 2014; Davis et al., 2014; Wilson et al., 2012). Streamflow seasonality follows the same gradient (Fig. 3d), with  
320 low seasonality around the Great Lakes where sandy aquifers sustain discharge year-round, and higher seasonality further  
321 SouthWest (Miller and White, 1998; Fig. 3d). A second gradient occurs in the MidWest from West to East, following  
322 precipitation and aridity gradients (Fig. S4). In the west, high aridity leads to high water balance losses to ET and low runoff  
323 coefficients at the annual and event scale (Fig. 3c).

324 **4.2.3 Region 3: West and Southwest**

325 The landscape of the West and Southwest region is dominated by the mountain ranges of the Coastal Ranges, Cascades, Sierra  
326 Nevada and Rocky Mountains, with mean watershed elevation ranging from 400 to over 2,700 meters. Dense populations in  
327 the coastal cities give way to sparsely populated inland areas. The climate exhibits strong gradients. The Pacific Northwest  
328 and Sierra Nevada mountain ranges receive substantial amount of precipitation than interior, with mean annual precipitation  
329 ranging from 460 to over 2,100 mm/yr across the region. The region shows a north-south temperature gradient with coastal  
330 moderation. Mean annual temperature ranges from 2°C in northern and high mountain areas to over 20°C in inland southern  
331 desert regions (Fig. S4). Precipitation patterns follow Mediterranean or semi-arid climates characterized by winter precipitation  
332 peaks and dry summers.

333

334 High baseflows with slow recession are prevalent across most of the Western region, where deep snowpacks drive sustained  
335 baseflow processes (Fig. 3a, S5; Barnhart et al., 2016; Tague and Grant, 2009). Inland areas tend to have faster recessions  
336 while retaining high baseflows, while coastal areas - where snow is rare - have lower baseflow while retaining slow recessions.  
337 The Southwest desert contrasts with the rest of the region, having low baseflows and fast recessions typical of the arid or semi-  
338 arid climate with water tables far below the land surface (Goodrich et al., 1997). Storage capacity and retention follow the  
339 same gradient from high in the Pacific Northwest to low in the South-East, but the high storage region is more constrained to  
340 the Rocky, Cascade and Sierra Nevada mountains (Fig. 3b). Water balance patterns contrast the pattern still further, with only  
341 the high mountains having high runoff ratios in contrast to low ratios throughout the remainder of the Western U.S. (Fig. 3c)  
342 Seasonal variability in processes is higher in the South (primarily California) where the seasonal Mediterranean climate pattern  
343 occurs with hot, dry summers and cool, wet winters (Fig. 3d, S5).

344

345 Processes in the coastal margin are markedly different from those inland. The moderating influence of the coast is strongly  
346 apparent in storage capacity (Fig. 3b): the northern Coast Ranges have lower average storage compared to high storage inland  
347 areas, while the southern coastal band has higher storage compared to low storage inland areas. Overland flows are strongly



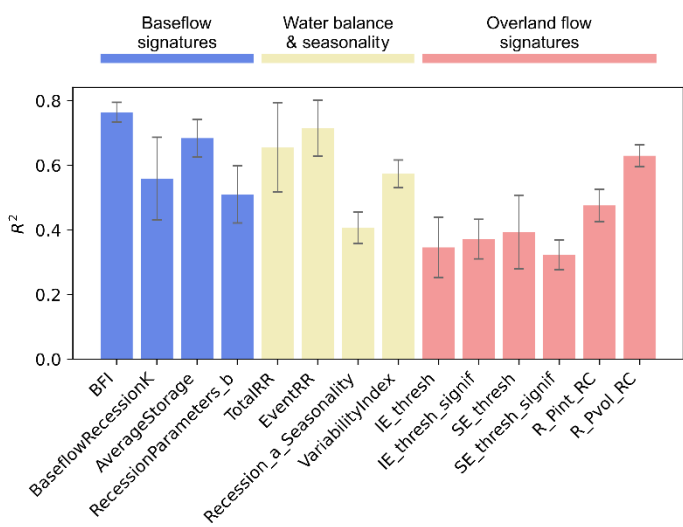
348 indicated all along the coast, but more weakly inland (Fig. 3e). Most overland flow favors saturation excess, although inland  
349 watersheds of the Southwest desert show areas of infiltration excess (Fig. 3f).

350 **4.3 Climate and landscape drivers of hydrologic processes**

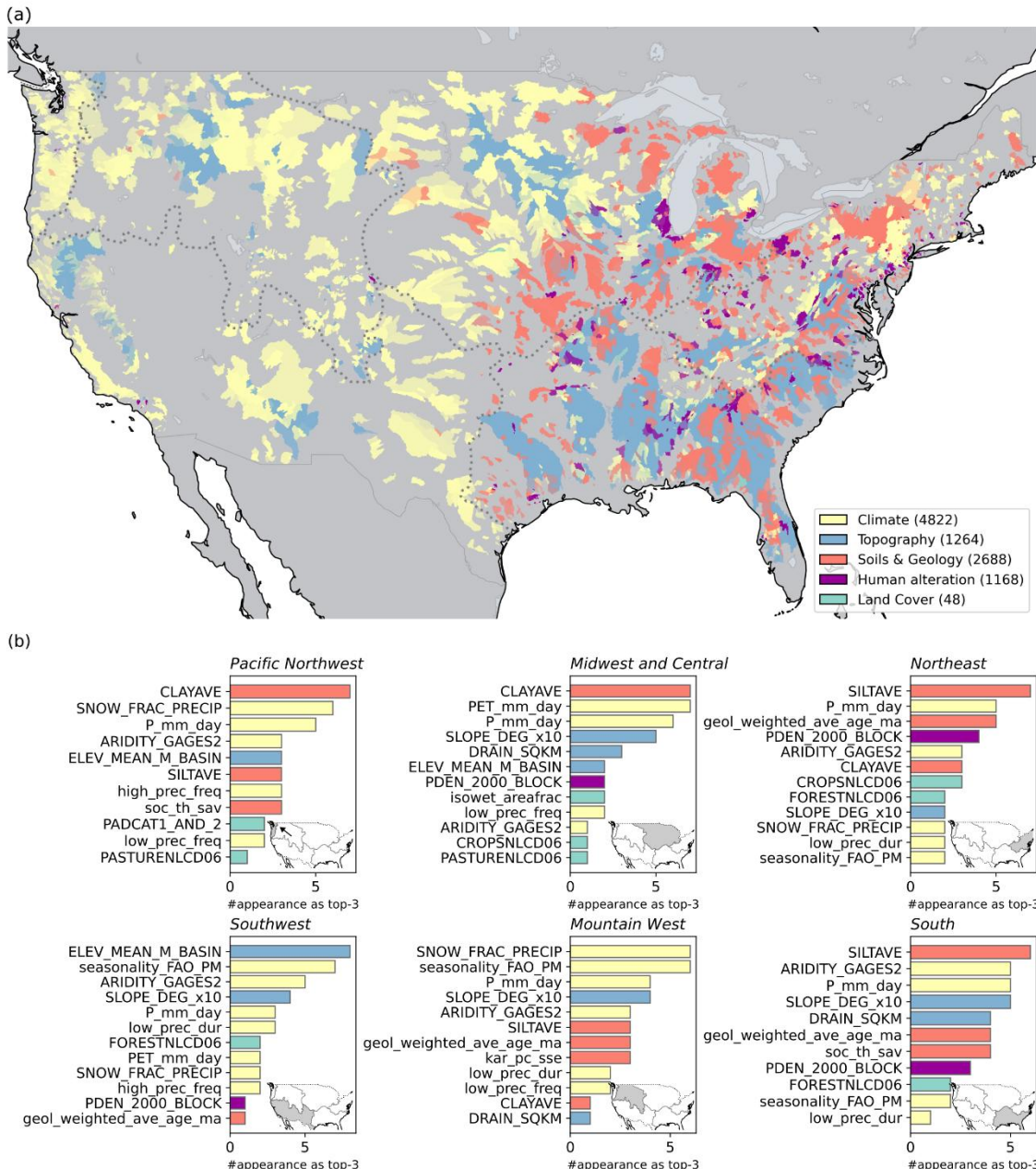
351 In this section, we interpret the random forest models to understand which aspects of climate and landscape are most important  
352 in controlling hydrologic processes in different regions of the U.S. Random forest models performed reasonably well ( $R^2 >$   
353 0.4) for most signatures (Fig. 5), consistent with previous studies using similar model setups (Addor et al., 2018; Beck et al.,  
354 2015; Bolotin and McMillan, 2024; Kuentz et al., 2017). Performance was higher for baseflow, water balance loss, and  
355 seasonality signatures, but lower for overland flow signatures. Figure S9 presents the regional model performances for each  
356 signature.

357

358 Figure 6 provides an overview of variable importance results: Figure 6a focuses on spatial patterns, showing the landscape  
359 attribute category that has the strongest contribution to predictions of signatures and processes for each watershed, calculated  
360 using aggregated Shapley values; Figures 6b provides deeper insights into the ranking of landscape attributes, ordered by  
361 permutation importance, for predicting signatures in each region. Figure S10 complements Figure 6a by showing the  
362 importance of landscape attribute categories in each region, based on permutation importance.



363  
364 **Figure 5: Ten-fold cross-validation performance of the random forest model trained on 4,748 CONUS-samples, where gauge IDs**  
365 **overlapped with Caravan and GAGES-II. Bars show the average  $R^2$  between observed and predicted signatures, with error bars**  
366 **representing the standard deviation. See Table 1 for signature names.**



367

368 **Figure 6: (a)** The landscape attribute category that contributes most to hydrologic responses was identified based on the average  
 369 relative contribution of each category,  $\bar{R}_k^{(y,i)}$  (derived from Shapley values; see Section 3.4). For each watershed, the most important  
 370 category  $k$  was determined using the median of  $\bar{R}_k^{(y,i)}$  across all hydrologic signatures. Results are displayed for the watershed  
 371 samples included in the random forest training. Numbers in the legend indicate the frequency that each category was identified as  
 372 the most important. (b) Frequency of watershed attributes ranked among the top three most important variables in permutation  
 373 importance (IncMSE%) across all signatures in six U.S. climate regions. The x-axis indicates how many times each attribute  
 374 appeared in the top three. See Section 3.4 and Table 2 for attribute names.



375 **4.3.1 Region 1: East and South**

376 In the East and South, a wide variety of landscape attribute categories dominate process predictions, including topography,  
377 soils and geology, climate and human alteration (Fig. 6). Climate attributes dominate in cooler areas in the Northeast and along  
378 the Appalachian spine, while topography attributes dominate on the Eastern coastal plain. Along the Gulf coast, either climate  
379 or soils and geology may dominate. Human alteration attributes dominate clusters of watersheds around cities including New  
380 York, Philadelphia, Washington D.C., Raleigh and Atlanta.

381

382 Overall, and particularly for signatures relating to storage and water balance in the East and South Region (*TotalRR*, *RR*  
383 *seasonality*, *Event RR*, *AverageStorage*, *RecessionParameters\_b*), the random forest models show that climate drivers are less  
384 important than in the rest of the U.S., and soils and geology land cover drivers are more important (Fig. 6, S10). Human  
385 influence (population density) is a more important driver here than in other regions across most signatures, consistent with  
386 large areas of high population (Fig. S7). For example, highly developed areas of Western Florida have anomalous areas of low  
387 baseflow, as do developed Piedmont areas (Zimmer and Gannon, 2018).

388

389 In the NorthEast, across all signatures, the drivers that most often appeared in the top three controls of random forest  
390 performance were Silt fraction, Precipitation, Geologic Age and Population density — representing the effects of geology,  
391 soils, climate and human development (Fig. 6b). Climate characteristics appear more often for signatures related to water  
392 balance and overland flow. In the South, Silt fraction, Aridity, Precipitation and Slope occur most often, representing gradients  
393 in elevation and soils from the Appalachians to the coastal plain and into Florida (Fig.s S6, S8).

394 **4.3.2 Region 2: MidWest and Central**

395 In the Midwest and Central area, a wide variety of landscape attribute categories dominate process predictions, including  
396 topography, soils and geology, climate and human alteration, showing strong spatial patterns (Fig. 6). Soils and geology  
397 attributes dominate in the Great Lakes region, and in the arc of clay-rich soils in the High Plains and Midwest regions (Fig.  
398 S6). A mixture of climate and topography attributes dominate in the Souris-Red-Rainy region. Human alteration attributes  
399 dominate in clusters of watersheds around Chicago, Detroit and Cleveland.

400

401 Overall in the Midwest and Central area, the random forest models show that land cover and topography drivers are more  
402 important than in the rest of the U.S., while climate drivers are less important. Across all signatures, the drivers that most often  
403 appeared in the top three controls of random forest performance were Clay fraction, PET, Precipitation and Slope —  
404 representing the effects of soils, climate and topography (Fig. 6). Despite the flat topography of the region, several topographic  
405 attributes appear in the top ten, perhaps reflecting the effect of unusual topographic features such as the driftless area. Land



406 cover metrics (wetland, cropland, pasture) were secondary drivers, appearing for signatures related to storage and overland  
407 flow.

408

409 The impact of climate is spread between multiple drivers: PET, Precipitation, Low precipitation frequency and Aridity. Climate  
410 drivers in the Midwest and Central area show multiple distinct spatial patterns, with aridity and low precipitation metrics  
411 showing an east-west gradient, temperature and PET having a north-south gradient, and precipitation and seasonality having  
412 a Northwest-Southeast gradient (Fig. S4, S5). Thus, each part of the Midwest and Central area has a unique holistic climate  
413 combination. Climate patterns differ distinctly from the NorthEast-Southwest pattern of the soils and land cover.

414 **4.3.3 Region 3: West and Southwest**

415 In the West, climate attributes dominate process predictions across most watersheds in the Pacific Northwest and Mountain  
416 West (Fig. 6a, S5). Some mountain areas have dominant topographic attributes, and topography drivers are more important in  
417 the Southwest region compared to the wider U.S.. Climate properties that appear most often include Snow fraction,  
418 Precipitation, Aridity and Seasonality (Fig. 6b: regions Pacific Northwest, Southwest, Mountain West). These attributes  
419 describe the primary climatic features of the West and Southwest U.S., which are governed by precipitation and aridity  
420 gradients from North to South, and from coasts to inland (Fig. S4). Inland mountain chains influence flow regimes by providing  
421 spring snowmelt and mountain block recharge, among the many influences of topography on hydrologic processes (Gnann et  
422 al., 2025). These controls are demonstrated by the importance of snow fraction alongside topographic attributes, elevation and  
423 slope. Soil control on runoff process is seen by the importance of clay fraction in the Pacific Northwest, reflecting Oregon's  
424 common clay soils (Miller and White, 1998).

425 **5 Discussion**

426 This study creates comprehensive maps of hydrologic processes across the contiguous United States by using machine learning  
427 to analyze streamflow signatures from over 10,000 watersheds and connecting these signatures to dominant watershed  
428 processes. The research reveals that climate primarily controls hydrologic processes in the western U.S., while soils and  
429 geology dominate in the Great Lakes region, topography controls processes in the Southeast, and human influences are most  
430 important around large cities across the East. The analysis shows distinct regional patterns in hydrologic processes, with  
431 infiltration excess overland flow dominating the high plains., saturation excess flow prevalent in the valleys of the Tennessee-  
432 Missouri region, and varying baseflow contributions across regions. These process maps provide novel information for  
433 selecting appropriate hydrologic models across large domains and help hydrologists anticipate how watersheds will respond  
434 to environmental changes such as altered climate or land use.



435 **5.1 New process understanding over large domains**

436 Our results build on previous work to map hydrologic processes and drivers. Our map of baseflow process importance shows  
437 similar patterns to previous studies into baseflow and groundwater contribution to streamflow (Beck et al., 2013; Santhi et al.,  
438 2008; Xie et al., 2024). As with those studies, our approach of using observations and machine learning methods provides finer  
439 detail than can be estimated using statistical interpolation or by hydrologic or climate models. By combining multiple recent  
440 datasets, we increase the number of observations used in our analysis. In our study, we used >10,000 observed watershed data  
441 within CONUS, representing a substantial advancement compared to the >600 to >3000 observation samples used in previous  
442 studies (Addor et al., 2018; Beck et al., 2013, 2015; Janssen and Ameli, 2021; Wu et al., 2021). Our analysis therefore provides  
443 a new benchmark, offering the most comprehensive coverage and highest spatial characterization of hydrologic processes  
444 across the contiguous United States to date. While larger datasets have been analyzed elsewhere, for example, >8,000  
445 watersheds (Santhi et al., 2008), >23,000 watersheds (Xie et al., 2024), those efforts focused exclusively on baseflow index.  
446 Beck et al. (2013) found sometimes differing drivers of baseflow index and recession slope despite their close connection: by  
447 using bivariate plots, we could more clearly highlight regions where patterns of these two signatures diverge. Those areas  
448 include the Pacific Northwest coast with lower baseflow index but slow recessions, and the central high plains with high  
449 baseflow index but fast recessions.

450

451 Previous studies investigated patterns of overland flow generation across the U.S. using soil maps and rainfall intensity  
452 (Buchanan et al., 2018) streamflow signatures (Wu et al., 2021) and modeling approaches (Wolock, 2003b). Like us, Buchanan  
453 et al. (2018) and Wu et al., (2021) found infiltration excess runoff important throughout the high plains, and saturation excess  
454 in the valleys of the Tennessee-Missouri region, and a mixture of saturation and infiltration excess in the Southwestern U.S..  
455 Substantial overland flow occurs in Southwest chaparral systems (Valeron and Meixner, 2010), and although deep groundwater  
456 tables suggest infiltration excess, we found a mixture of mechanisms. This could be due to incorrect inference: where  
457 magnitude of overland flow is related to storm size rather than intensity, as smaller storms are intercepted by the dense canopy,  
458 signatures may incorrectly assign this runoff to saturation excess flow. However, our results are supported by global studies  
459 that show saturation excess is always more common than infiltration excess even in arid regions, as saturation excess is  
460 generated in riparian zones and topographic convergence areas where water tables are higher (McMillan et al., 2025).

461

462 By mapping and categorizing the primary drivers of runoff processes, we can untangle which physical characteristics drive the  
463 hydrologic response in each region. In some areas, there are multiple landscape attributes that could contribute to the response,  
464 for example in the Gulf Coast region the speed of recessions might be reduced by the high depth to bedrock, but increased by  
465 soils with low hydraulic conductivity. We find that silt fraction (soil texture) drives the response, creating fast recessions, with  
466 mapping showing that this is most important along the coastal margin. Our maps of primary drivers based on Shapley values  
467 extend previous work to analyze the drivers of hydrologic signatures. For example, Addor et al. (2018; their Fig. 3) show that



468 climate (aridity, seasonality, snow fraction) is the primary driver across most signatures, with topography (elevation, slope)  
469 and land cover (forest, leaf area index) being secondary drivers. Figure 6a similarly shows climate and topography as dominant,  
470 but adds spatial information to show that, for example, climate is dominant in the mountainous western U.S., but soils and  
471 geology dominate the Midwest and much of the Northeastern U.S. Geological age, a recently-proposed attribute to summarize  
472 watershed geology, was often in the top random forest attributes (Holt and McMillan, 2025). This highlights the need and  
473 opportunity for development of new landscape attributes that characterize the subsurface, echoing the call by Tarasova et al.  
474 (2023).

## 475 5.2 Informing model selection and evaluation

476 Our results support hydrological modeling by enabling hydrologists to check whether key processes in a watershed are well-  
477 represented by a candidate model prior to application. A wide range of hydrologic models with differing process  
478 representations, structures and complexities are available (Knoben et al., 2020). Hydrologists must make choices on whether  
479 to include simulations of additional processes such as snowpack or deep groundwater, and the complexity required such as  
480 including energy balance at the land surface. Our maps of hydrologic processes provide a pre-screening tool to match  
481 hydrological models with appropriate process representations to regions. This approach aims to reduce model structural errors  
482 by discouraging use of models ill-suited to the dominant processes (e.g., using a bucket model in overland flow-dominated  
483 regions).

484

485 Many previous studies have assessed preferred model structure in individual research watersheds, often using in-depth data  
486 analysis to ensure that modeled processes are consistent with observed processes (e.g. Hrachowitz et al., 2014; Kavetski and  
487 Fenicia, 2011). This study provides a method to support transparent model justification in applied studies without the resources  
488 to conduct model structure investigations, and to upscale model structure decisions to large domains. For example, if selecting  
489 models from the MARRMoT toolbox (Knoben et al., 2020), models for regions of dominant overland flow should include  
490 saturation excess and/or infiltration excess pathways, and models for regions of complex storage and retention should include  
491 multiple parallel groundwater reservoirs. The ability to choose appropriate models for thousands of watersheds is needed for  
492 new, flexible model frameworks such as the U.S. Next-Generation National Water Model Framework (Cosgrove et al., 2024;  
493 Johnson et al., 2023; Ogden et al., 2021). Our observation-based method complements previous large-domain model-based  
494 methods that use analysis of model sensitivities (Markstrom et al., 2016) and performance (Prieto et al., 2021; Spieler et al.,  
495 2020) Therefore, where hydrologists seek to evaluate models against process representation, this study offers an opportunity  
496 to enhance model benchmarking frameworks by adding process realism as a metric.

## 497 5.3 Limitations and future work

498 The hydrologic process maps produced by this study are limited to the contiguous U.S.. Recent streamflow observation datasets  
499 offer the opportunity to extend this method to other regions or globally. Such datasets include the community Caravan dataset



500 (Kratzert et al., 2023), and the international dataset of watersheds with limited human influences, Reference Observatory of  
501 Basins for International hydrological climate change detection (ROBIN; Turner et al., 2025). If extending the method globally,  
502 caution is advised with scaling, in order to represent different ranges of signature values in different regions. In this study, we  
503 plotted signature values as quantiles based on the U.S. distribution, but other countries may have very different signature  
504 distributions (McMillan et al., 2022). Therefore, watershed processes that are considered important in a U.S. context, may be  
505 considered less important in a global context. Further, some regions of the U.S. are excluded or poorly represented in the  
506 dominant process maps presented in this paper, due to a low spatial coverage of USGS stream gages. For example, there are  
507 significant gaps in the arid southwest where perennial streamflow is rare (Kiang et al., 2013; Krabbenhoft et al., 2022). In such  
508 regions there is a need for alternative process-mapping methods that do not rely on streamflow records.

509

510 A limitation of this study that would become more apparent at a global scale is the quality of precipitation, streamflow, and  
511 attribute data. A previous study noted issues with limited quality and consistency of the global attribute data for soils and  
512 geology that reduced their predictive power (Beck et al., 2015). Continental scales necessitate the use of gridded precipitation  
513 products, but in areas with low density of observations these products may be insufficient to analyze localized, flashy processes  
514 such as infiltration excess flow (McMillan et al., 2023). In small, headwater watersheds, precipitation grid size may be large  
515 compared to watershed area, and headwaters are also underrepresented in streamflow observations (Golden et al., 2025). In  
516 snowy areas, signature values can be compromised because liquid water inputs to the watershed come from snowmelt rather  
517 than directly from precipitation. In our study, we excluded snow-dominated watersheds for signatures related to overland flow,  
518 as these require event-scale surface water input that are particularly affected by frozen or snowmelt conditions. Products such  
519 as NLDAS3 (Case et al., 2025) or surface water inputs considering rain-on-snow and snowmelt (Hammond, 2024; Hammond  
520 and Kampf, 2020) may provide future abilities to estimate overland flow processes in snow areas using estimates of hourly  
521 snow accumulation and melt. While our study used potential evapotranspiration (PET) information in only one signature  
522 (*AverageStorage*), uncertainty in PET is a major issue of global datasets and needs to be addressed (Clerc-Schwarzenbach et  
523 al., 2024; Destouni and Zarei, 2024) before this approach can be expanded to a variety of (eco)hydrologic processes.

524

525 A further limitation is the extent to which continental scale maps of dominant processes can be validated. Large-domain  
526 signature datasets can be evaluated for data quality, for interpolation quality using cross-validation, and compared with  
527 previous datasets. However, it is more difficult to determine how accurately signatures relate to processes over large domains.  
528 Research watersheds offer “ground truth” points at which processes are already well understood (Penna, 2024). Previous  
529 studies used a handful of U.S. critical zone observatory watersheds for evaluation (McMillan et al., 2022). However, the large  
530 number of past and present research watersheds across the globe offer an interesting future opportunity for wider-scale  
531 validation of process mapping techniques (McMillan et al., 2025; Sebestyen et al., 2025). Similarly, validation of process  
532 drivers remains challenging. While Shapley values and permutation importance provide explanatory power for random forest  
533 models, they have some limitations. Both metrics characterize model interactions within a given dataset; therefore, the variety



534 of processes covered in the dataset matters, and data or model uncertainties may propagate into the interpretations (Husic,  
535 Shapley values do not capture joint distributional effects among multiple interacting variables (Lundberg and Lee,  
536 2017). Developing an explanatory framework that maximizes both model performance and interpretability remains an ongoing  
537 research area in hydrology (Robert Maier et al., 2024; Willard et al., 2024).

## 538 **5 Conclusion**

539 A fundamental question in hydrology is how hydrologic processes are organized over large scales, and how they are controlled  
540 by climate and landscape (Blöschl et al., 2019). In this study, we contribute towards answering this question by mapping  
541 hydrologic processes and their drivers across the contiguous U.S.. Our approach used hydrologic signatures to describe  
542 streamflow dynamics, and connected these dynamics to dominant processes in the associated watersheds using established  
543 relationships between signatures and watershed processes. We analyzed 14,146 gauged U.S. watersheds; our map of processes  
544 was based on observational data from 10,261 gauged sites and extended using random forest predictions to an additional 3,885  
545 watersheds with insufficient record length or completeness. Our method enables knowledge transfer from gauged basins with  
546 well-established conceptual models to ungauged or poorly instrumented watersheds.

547

548 Our results comprise maps of hydrologic process importance across the contiguous U.S., including baseflow, overland flow,  
549 water storage, seasonal variation and water balance processes. Using interpretable machine learning methods, we create maps  
550 of process drivers that explain which climate and landscape attributes are dominant in controlling hydrologic processes in each  
551 watershed and each region. We find clear patterns at the continental scale, such that processes most strongly relate to climate  
552 in the western U.S., to soils and geology in the Great Lakes region, to topography in the Southeast, and to human influences  
553 around large cities, especially in the Northeast.

554

555 Our findings extend and generalize process understanding from research watersheds to large domains, revealing regional  
556 heterogeneity within broader physiographic provinces that are often treated as hydrologically uniform. Hydrologic process  
557 maps provide essential support for new, large-domain model frameworks that must select model structure across thousands of  
558 watersheds. These maps enable hydrologists to select models that adequately represent the dominant processes of a watershed.  
559 Identification of dominant processes in each region further enables hydrologists to anticipate streamflow response to  
560 environmental change, by identifying which processes are most sensitive to shifts in driving variables. Such analysis has the  
561 potential to support scenario testing for future land use or climate, to guide selection of green and grey infrastructure compatible  
562 with dominant processes, and to inform risk assessments for regions prone to flash flooding, streamflow depletion, or altered  
563 seasonal flow regimes.



## 564 Code availability

565 Code used for analysis is available via Zenodo at (*The Zenodo link will be made available following the revision and upon*  
566 *completion of the publication-ready version*) and as a continuously updated version via GitHub at  
567 <https://github.com/RY4GIT/signature-prediction>. Code used to calculate geologic and wetland attributes (Holt and McMillan,  
568 2025) is deposited in Zenodo at (*The Zenodo link will be made available following the revision and upon completion of the*  
569 *publication-ready version*) and as a continuously updated version via GitHub at  
570 [https://github.com/RY4GIT/Wetland\\_GeologicAge\\_Attributes](https://github.com/RY4GIT/Wetland_GeologicAge_Attributes). Caravan attributes for GAGES-II only watersheds were  
571 calculated using <https://github.com/kratzert/Caravan> (Kratzert et al., 2023). Hydrologic signatures are calculated using  
572 <https://github.com/RY4GIT/TOSSH>, which modified the original TOSSH toolbox <https://github.com/TOSSHtoolbox/TOSSH>  
573 (Gnann et al., 2021b).

## 574 Data availability

575 The hydrologic signature datasets, derived from observed data and predicted using random forest models, are deposited at (*The*  
576 *Hydroshare link will be made available following the revision and upon completion of the publication-ready version*). The  
577 Caravan Version 1.5 dataset is available at <https://doi.org/10.5281/zenodo.10968468> (Kratzert et al., 2024), which contains  
578 streamflow, meteorological data, watershed boundaries and attributes. GAGES-II attributes are available at  
579 <https://www.sciencebase.gov/catalog/item/631405bb34e36012efa304a> (Falcone, 2011), and time series of meteorological  
580 data for GAGES-II locations are available from <https://www.sciencebase.gov/catalog/item/64134069d34eb496d1ce3c6f>  
581 (Wieczorek et al., 2023) and <https://www.sciencebase.gov/catalog/item/6494515fd34ef77fcb014eb0> (Hammond, 2024).  
582 CAMELSH hourly NLDAS forcings are available at <https://doi.org/10.5281/zenodo.15066778> and  
583 <https://doi.org/10.5281/zenodo.15070091> (Tran et al., 2025).

## 584 Author contribution

585 **Araki:** conceptualization, data curation, formal analysis, investigation, methodology, software, visualization, writing –  
586 original draft preparation, writing – review and editing. **Holt:** conceptualization, data curation, methodology, software, writing  
587 – review and editing. **Hammond:** data curation, formal analysis, methodology, writing – original draft preparation, writing  
588 – review and editing. **Husic:** formal analysis, investigation, methodology, writing – original draft preparation, writing –  
589 review and editing. **Coxon:** investigation, writing – review and editing. **McMillan:** funding acquisition, project administration,  
590 conceptualization, formal analysis, investigation, methodology, writing – original draft preparation, writing – review and  
591 editing, supervision.



592 **Competing interests**

593 At least one of the (co-)authors is a member of the editorial board of Hydrology and Earth System Sciences. The peer-review  
594 process was guided by an independent editor, and the authors also have no other competing interests to declare.

595 **Acknowledgement**

596 We thank Sebastian Gnann for the development of the TOSSH toolbox and for the collaborative discussions around my pull  
597 requests, and Yueling Ma for helpful input on interpretable Machine Learning methods during a conference. The bivariate map  
598 was inspired by a blogpost written by Muhammad Mohsin Raza on their website DataWim. We thank Roy Sandro and Scott  
599 Hamshaw for helpful feedback on the earlier version of the manuscript. We appreciate the computing support provided by the  
600 IT team at the Department of Geography, San Diego State University, and the General Research IT (GRIT) team at the  
601 University of California, Santa Barbara. Any use of trade, firm, or product names is for descriptive purposes only and does not  
602 imply endorsement by the U.S. government.

603 **Financial Support**

604 Araki, Holt, McMillan were supported by the NSF Hydrologic Sciences Program, Division of Earth Sciences, Award Number  
605 2124923. Araki acknowledges support from the Shida Scholarship Program. Coxon was supported by a UKRI Future Leaders  
606 Fellowship [MR/V022857/1].

607



608 **Tables**

609 **Table 1:** Hydrologic signatures used for building process hypotheses. The signature descriptions are adapted from  
 610 (McMillan et al., 2022).

Hydrologic processes and signature hypothesis	Relationship between the signature values and process strength	Signature	Unit	Description
<b>Baseflow</b>  We hypothesize that a larger baseflow magnitude (i.e., higher <i>BFI</i> ) and a slower recession rate (i.e., lower <i>BaseflowRecessionK</i> ) indicate a stronger baseflow process.	Positive	<i>BFI</i>	-	Baseflow index (BFI) represents baseflow proportion and residence time (Bulygina et al., 2009; Yilmaz et al., 2008). Calculated as mean baseflow divided by mean streamflow. Hydrograph separation is implemented to obtain baseflow fraction using the UKIH smoothed minima method (UKIH, 1980).
	Negative	<i>BaseflowRecessionK</i>	1/d	Represents groundwater influence and longer subsurface flow paths (Safeeq et al., 2013). Calculated as an exponential recession constant K fitted to the master recession curve derived from adaptive matching strip method.
<b>High storage capacity</b>  We hypothesize that larger storage (i.e., higher <i>AverageStorage</i> ) and more nonlinear recession behavior (i.e., higher <i>RecessionParameters_b</i> ) indicate a greater storage capacity and the involvement of multiple storages.	Positive	<i>AverageStorage</i>	mm	Represents average magnitude of watershed storage (Peters and Aulenbach, 2011). Derived from average baseflow and storage-discharge relationship. Uses a simple water balance model to calculate changes in storage, then finds the relationship between storage and discharge, and then estimates average storage from average baseflow.
	Positive	<i>RecessionParameters_b</i>	-	The nonlinearity indicates the contributions of multiple storages (Clark et al., 2009; Tallaksen, 1995). Recession analysis parameters approximate storage-discharge relationship. Fits a line to the $dQ/dt$ -Q relationship in log-log space for each individual recession and returns the median slope. b is a shape parameter representing the degree of nonlinearity.
<b>Water balance losses</b>  We hypothesize that a smaller runoff ratio (Q:P ratio) at both interannual and event scales (i.e., lower <i>TotalRR</i> and <i>EventRR</i> ) indicates greater water balance losses due to evapotranspiration, deep drainage to groundwater, or some other processes.	Negative	<i>TotalRR</i>	-	Total runoff ratio (RR) infer evapotranspiration or other flow bypassing gauge (Safeeq and Hunsaker, 2016). Calculated as mean streamflow divided by mean precipitation.
	Negative	<i>EventRR</i>	-	Event runoff ratio (RR) infer rapid vertical drainage of water to groundwater (Noguchi et al., 1997). Calculated as an average of runoff ratios (streamflow divided by precipitation) from all identified storm events.



<b>Seasonal variability</b>  We hypothesize that greater flow variability, both in general patterns (i.e., higher <i>Variability Index</i> ) and in seasonal patterns (i.e., higher <i>Recession_a_Seasonality</i> ), indicates a stronger influence of seasonal evapotranspiration patterns on water storage.	Positive	<i>Recession_a_Seasonality</i>	-	Seasonal variation in the recession “a” parameter reflects the impact of evapotranspiration on water storage (Shaw and Riha, 2012). Calculated as the difference between the maximum and minimum monthly median values of the y-intercept (“a” parameter) in the $dQ/dt - Q$ relationship in log-log space, assuming a slope of 2.
	Positive	<i>VariabilityIndex</i>	-	High variability index shows lower water storage (Estrany et al., 2010). Calculated as the standard deviation of log-transformed discharge values determined at 10% intervals from 10% to 90% of the cumulative frequency distribution (flow duration curve).
<b>Overland flow</b>  We hypothesized that a strong threshold relationship between quickflow and precipitation characteristics (i.e., high significance and higher threshold values) suggests a more dominant overland flow process.	Negative (Values outside the range $0 \leq P\text{-value} \leq 0.05$ are deemed insignificant and clipped out. Within the range, the smaller P-value is, the more significant the threshold is)	<i>Average of IE_thresh_sig and SE_thresh_si gnif</i>	-	Significant values ( $<0.05$ ) imply infiltration excess (IE) or saturation excess (SE) occurs (Ali et al., 2013; McGrath et al., 2007). <i>p</i> -value was calculated for the significance of a non-zero change in slope above and below a threshold in a relationship of event quickflow volume versus event maximum precipitation intensity (for IE) or event total precipitation volume (for SE).
	Positive	<i>Average of IE_thresh and SE_thresh</i>	mm	Indicates rainfall intensity or event precipitation depth required to generate infiltration excess or saturation excess, respectively (Ali et al., 2013; McGrath et al., 2007). Value of the threshold identified in the IE/SE_thresh_signif signature. The “broken-stick” model was fit to the relationship between quickflow vs. precipitation characteristics.
<b>Overland flow type</b>  We hypothesized that the relative strength in infiltration vs. saturation of excess overland flow (i.e., differences in <i>RC_Pvol</i> and <i>RC_Pint</i> ) indicate the prevalence of either overland flow mechanisms.  Exclude watersheds where event runoff coefficient has negative relationships with storm characteristics (i.e., $RC\_Pvol < 0$ and $RC\_Pint < 0$ ).	Positive relationship with infiltration excess overland flow	<i>RC_Pvol</i>	-	Indicates stormflow processes sensitive to rainfall intensity, for example, infiltration excess (Hortonian) overland flow (Wu et al., 2021). Calculated as the Spearman correlation coefficients between event runoff coefficient and event maximum rainfall intensity. As per (Wu et al., 2021), event maximum rainfall intensity is calculated as the multiplication of daily rainfall (mm/day) from original climate forcings (i.e., ERA5 for Caravan, gridMET for GAGES-II) multiplied by the fraction of maximum rainfall intensity from CAMELSh hourly NLDAS forcings.
	Positive relationship with saturation excess overland flow	<i>RC_Pint</i>	-	Indicates stormflow processes sensitive to rainfall volume, for example, saturation excess overland flow, subsurface stormflow, and groundwater flow (Wu et al., 2021). Calculated as the Spearman correlation coefficients between event runoff coefficient and rainfall volume.



613 **Table 2:** Landscape attributes used in training the random forest model. Descriptions are adapted from (Falcone, 2011;  
 614 Falcone et al., 2010; Holt and McMillan, 2025; Kratzert et al., 2023; Linke et al., 2019). For predictions, when certain  
 615 attributes are unavailable, equivalent attributes are substituted (e.g., Caravan equivalents are used when predicting signatures  
 616 for watershed samples available only in Caravan). The combinations are detailed in Table S1. An asterisk (\*) in the unit  
 617 column indicates that the landscape attribute unit from GAGES-II was converted to the Caravan equivalent (Fig. S11 shows  
 618 the comparison).  
 619

Category	Attribute Name	Description	Unit	Original Source	Dataset Source	Caravan Equivalent
Physiography	ELEV_MEA_N_M_BASIN	Mean watershed elevation	meters	USGS 100m National Elevation Dataset (Gesch et al., 2018)	GAGES-II	ele_mt_sav
Physiography	DRAIN_SQ_KM	Watershed drainage area	km <sup>2</sup>	Multiple sources, while the majority derived from NHDPlus (U.S. Environmental Protection Agency, 2008) (see original USGS, 2011 report on GAGES-II)	GAGES-II	area
Physiography	SLOPE_PCT	Mean watershed slope, percent	%	USGS 100m resolution National Elevation Dataset (Gesch et al., 2018)	GAGES-II	slp_dg_sav
Land Cover	FORESTNL_CD06	Forest extent	% area	NLCD06 for most regions; NLCD01 for Alaska, Hawaii, and Puerto Rico (Yang et al., 2018)	GAGES-II	for_pc_sse
Land Cover	CROPSNLC_D06	Cultivated Crops extent	% area		GAGES-II	crp_pc_sse
Land Cover	PASTURENL_LCD06	Pasture/Hay extent	% area		GAGES-II	pst_pc_sse
Land Cover	PCT_IRRIG_AG	Irrigated agriculture extent	% area	Based on 250m MODIS datasets, USGS MiRAD-US (Shrestha et al., 2019)	GAGES-II	ire_pc_sse
Land Cover	PADCAT1_AND_2	Percent of watershed designated as Protected Area Category 1 and 2	% area *	Protected Areas Database (United States Geological Survey, 2024)	GAGES-II	pac_pc_sse



Land Cover	isowet_areafra	Isolated wetland area fraction (Holt, 2024)	-	National Wetlands Inventory (Lane and D'Amico, 2016)	Holt and McMillan, 2025	N/A
Soils & Geology	CLAYAVE	Average clay content	%	STATSGO (United States Department of Agriculture et al., 2008)	GAGES-II	cly_pc_sav
Soils & Geology	SILTAVE	Average silt content	%		GAGES-II	slt_pc_sav
Soils & Geology	soc_th_sav	Organic carbon content in soil	tonnes/hectare		Caravan/HydroAtlas	N/A
Soils & Geology	kar_pc_sse	Karst area extent	% area	Rock Outcrops v3.0 (Williams and Ford, 2006)	Caravan/HydroAtlas	N/A
Soils & Geology	geol_weighted_ave_age_ma	Area-weighted average of geologic age	ma	The USGS State Geologic Map Compilation (Horton et al., 2017)	Holt and McMillan, 2025	N/A
Anthropogenic	PDEN_2000_BLOCK	Population density in the watershed	persons /km <sup>2</sup>	2000 Census block data regridded to 100m	GAGES-II	ppd_pk_sav
Climate	P_mm_day	Mean annual precipitation (1971-2000). The unit was converted from the original variable “PPTAVG_BASIN” in cm/year to mm/day.	mm/day *	800m PRISM data	GAGES-II	p_mean
Climate	PET_mm_day	Mean annual potential evapotranspiration rate estimated from mean monthly air temperature and latitude using Hamon (1961) equation. The unit was converted from the original variable “PET” in mm/year to mm/day.	mm/day *	Monthly air temperature from 30-year (1961-1990) PRISM	GAGES-II	pet_mean_FAO_PM
Climate	ARIDITY_GAGES2	Aridity index, ratio of mean PET and mean precipitation	-	Calculated from PPTAVG_BASIN and PET in GAGES-II attributes	GAGES-II	aridity_FAO_PM
Climate	SNOW_PCT_PRECIP	Mean snow percent of total precipitation estimate (1901-2000)	- *	McCabe and Wolock (submitted, 2008), 1km grid	GAGES-II	frac_snow



Climate	seasonality_F_AO_PM	Moisture index seasonality in range [0, 2] (Knoben et al., 2018), where 0 indicates no change in the water or energy budget throughout the year, and 2 indicates a transition from fully arid to fully humid conditions. The moisture index is calculated as the normalized aridity index at the monthly scale.	-	ERA-5 (Muñoz Sabater, 2019); The FAO Penman–Monteith equation (Allen et al., 1998; Shalev and Kratzert, 2024) is used to calculate Potential Evapotranspiration (PET)	Caravan/ERA-5	N/A
Climate	high_prec_freq	Frequency of high precipitation days, where precipitation $\geq 5$ times mean daily precipitation	-	ERA-5 (Muñoz Sabater, 2019)	Caravan/ERA-5	N/A
Climate	low_prec_freq	Frequency of low precipitation days, where precipitation $< 1$ mm/day	-	ERA-5 (Muñoz Sabater, 2019)	Caravan/ERA-5	N/A
Climate	low_prec_dur	Average duration of low precipitation events (number of consecutive days where precipitation $< 1$ mm/day)	day	ERA-5 (Muñoz Sabater, 2019)	Caravan/ERA-5	N/A

620 **References**

621 Abban, B., Papanicolaou, A. N. (thanos), Cowles, M. K., and Wilson, C. G.: Examining Seasonal Trends in Sediment Source  
622 Contributions in an Intensely Cultivated Midwestern Sub-Watershed Using Bayesian Unmixing, in: World Environmental and  
623 Water Resources Congress 2014, World Environmental and Water Resources Congress 2014, Portland, Oregon, 1453–1463,  
624 https://doi.org/10.1061/9780784413548.146, 2014.

625 Addor, N., Newman, A. J., Mizukami, N., and Clark, M. P.: The CAMELS data set: catchment attributes and meteorology for  
626 large-sample studies, Hydrol. Earth Syst. Sci., 21, 5293–5313, https://doi.org/10.5194/hess-21-5293-2017, 2017.

627 Addor, N., Nearing, G., Prieto, C., Newman, A. J., Le Vine, N., and Clark, M. P.: A ranking of hydrological signatures based  
628 on their predictability in space, Water Resour. Res., 54, 8792–8812, https://doi.org/10.1029/2018WR022606, 2018.

629 Ali, G., Tetzlaff, D., Soulsby, C., McDonnell, J. J., and Capell, R.: A comparison of similarity indices for catchment  
630 classification using a cross-regional dataset, Adv. Water Resour., 40, 11–22, https://doi.org/10.1016/j.advwatres.2012.01.008,  
631 2012.

632 Ali, G., Oswald, C. J., Spence, C., Cammeraat, E. L. H., McGuire, K. J., Meixner, T., and Reaney, S. M.: Towards a unified  
633 threshold-based hydrological theory: necessary components and recurring challenges: INVITED COMMENTARY, Hydrol.  
634 Process., 27, 313–318, https://doi.org/10.1002/hyp.9560, 2013.



635 Allen, R. G., Pereira, L. S., Raes, D., and Smith, M.: Crop Evapotranspiration – Guidelines for Computing Crop Water  
636 Requirements, in: FAO Irrigation and drainage paper 56, Food and Agriculture Organization of the United Nations, Rome,  
637 Italy, 1998.

638 Almagro, A., Meira Neto, A. A., Vergopolan, N., Roy, T., Troch, P. A., and Oliveira, P. T. S.: The Drivers of Hydrologic  
639 Behavior in Brazil: Insights From a Catchment Classification, Water Resources Research, 60,  
640 <https://doi.org/10.1029/2024WR037212>, 2024.

641 Angermann, L., Jackisch, C., Allroggen, N., Sprenger, M., Zehe, E., Tronicke, J., Weiler, M., and Blume, T.: Form and function  
642 in hillslope hydrology: characterization of subsurface flow based on response observations, *Hydrol. Earth Syst. Sci.*, 21, 3727–  
643 3748, <https://doi.org/10.5194/hess-21-3727-2017>, 2017.

644 Araki, R., Branger, F., Wiekenkamp, I., and McMillan, H. K.: A signature-based approach to quantify soil moisture dynamics  
645 under contrasting land-uses, *Hydrol. Process.*, 36, e14553, <https://doi.org/10.1002/hyp.14553>, 2022.

646 Ariano, S. and Ali, G.: From river flow regime diversity to proxies for hydrologic homogeneity a Canada-wide case study, *Sci.  
647 Rep.*, 15, 16743, <https://doi.org/10.1038/s41598-025-00244-7>, 2025.

648 Arsenault, R., Brissette, F., Martel, J.-L., Troin, M., Lévesque, G., Davidson-Chaput, J., Gonzalez, M. C., Ameli, A., and  
649 Poulin, A.: A comprehensive, multisource database for hydrometeorological modeling of 14,425 North American watersheds,  
650 *Sci Data*, 7, 243, <https://doi.org/10.1038/s41597-020-00583-2>, 2020.

651 Barnhart, T. B., Molotch, N. P., Livneh, B., Harpold, A. A., Knowles, J. F., and Schneider, D.: Snowmelt baseflow  
652 contributions: A comparison of methods using nested catchments in the Colorado River basin, *Water Resources Research*, 52,  
653 4524–4548, 2016.

654 Barnhart, T. B., Farmer, W. H., Hammond, J. C., Sexstone, G. A., Curran, J. H., Koch, J. C., and Driscoll, J. M.: Evaluating  
655 hydrologic region assignment techniques for ungaged basins in Alaska, USA, *River Res. Appl.*, 38, 1569–1584,  
656 <https://doi.org/10.1002/rra.4028>, 2022.

657 Beck, H., Dijk, A., Miralles, D., Jeu, R. A. M., (Sampurno) Bruijnzeel, L., McVicar, T., and Schellekens, J.: Global patterns  
658 in base flow index and recession based on streamflow observations from 3394 catchments, *Water Resources Research*, 49,  
659 7843–7863, <https://doi.org/10.1002/2013WR013918>, 2013.

660 Beck, H. E., De Roo, A., and van Dijk, A. I.: Global maps of streamflow characteristics based on observations from several  
661 thousand catchments, *J. Hydrometeorol.*, 16, 1478–1501, 2015.

662 Berghuijs, W. R., Sivapalan, M., Woods, R. A., and Savenije, H. H. G.: Patterns of similarity of seasonal water balances: A  
663 window into streamflow variability over a range of time scales, *Water Resour. Res.*, 50, 5638–5661,  
664 <https://doi.org/10.1002/2014WR015692>, 2014.

665 Blöschl, G.: Hydrologic synthesis: Across processes, places, and scales, *Water Resour. Res.*, 42,  
666 <https://doi.org/10.1029/2005wr004319>, 2006.

667 Blöschl, G., Bierkens, M. F. P., Chambel, A., Cudennec, C., Destouni, G., Fiori, A., Kirchner, J. W., McDonnell, J. J., Savenije,  
668 H. H. G., Sivapalan, M., Stumpf, C., Toth, E., Volpi, E., Carr, G., Lupton, C., Salinas, J., Széles, B., Viglione, A., Aksoy, H.,



669 Allen, S. T., Amin, A., Andréassian, V., Arheimer, B., Aryal, S. K., Baker, V., Bardsley, E., Barendrecht, M. H., Bartosova,  
670 A., Batelaan, O., Berghuijs, W. R., Beven, K., Blume, T., Bogaard, T., Borges de Amorim, P., Böttcher, M. E., Boulet, G.,  
671 Breinl, K., Brilly, M., Brocca, L., Buytaert, W., Castellarin, A., Castelletti, A., Chen, X., Chen, Y., Chen, Y., Chifflard, P.,  
672 Claps, P., Clark, M. P., Collins, A. L., Croke, B., Dathe, A., David, P. C., de Barros, F. P. J., de Rooij, G., Di Baldassarre, G.,  
673 Driscoll, J. M., Duethmann, D., Dwivedi, R., Eris, E., Farmer, W. H., Feiccabruno, J., Ferguson, G., Ferrari, E., Ferraris, S.,  
674 Fersch, B., Finger, D., Foglia, L., Fowler, K., Gartsman, B., Gascoin, S., Gaume, E., Gelfan, A., Geris, J., Gharari, S., Gleeson,  
675 T., Glendell, M., Gonzalez Bevacqua, A., González-Dugo, M. P., Grimaldi, S., Gupta, A. B., Guse, B., Han, D., Hannah, D.,  
676 Harpold, A., Haun, S., Heal, K., Helffricht, K., Herrnegger, M., Hipsey, M., Hlaváčiková, H., Hohmann, C., Holko, L.,  
677 Hopkinson, C., Hrachowitz, M., Illangasekare, T. H., Inam, A., Innocente, C., Istanbulluoglu, E., Jarihani, B., et al.: Twenty-  
678 three unsolved problems in hydrology (UPH) – a community perspective, *Hydrol. Sci. J.*, 64, 1141–1158,  
679 <https://doi.org/10.1080/02626667.2019.1620507>, 2019.  
680 Bolotin, L. A. and McMillan, H.: A hydrologic signature approach to analysing wildfire impacts on overland flow, *Hydrol.*  
681 *Process.*, 38, <https://doi.org/10.1002/hyp.15215>, 2024.  
682 Bracken, L. J., Wainwright, J., Ali, G. A., Tetzlaff, D., Smith, M. W., Reaney, S. M., and Roy, A. G.: Concepts of hydrological  
683 connectivity: Research approaches, pathways and future agendas, *Earth-Sci. Rev.*, 119, 17–34,  
684 <https://doi.org/10.1016/j.earscirev.2013.02.001>, 2013.  
685 Brooks, P. D., Chorover, J., Fan, Y., Godsey, S. E., Maxwell, R. M., McNamara, J. P., and Tague, C.: Hydrological partitioning  
686 in the critical zone: Recent advances and opportunities for developing transferable understanding of water cycle dynamics:  
687 CRITICAL ZONE HYDROLOGY, *Water Resour. Res.*, 51, 6973–6987, <https://doi.org/10.1002/2015wr017039>, 2015.  
688 Brunner, M. I., Melsen, L. A., Newman, A. J., Wood, A. W., and Clark, M. P.: Future streamflow regime changes in the United  
689 States: assessment using functional classification, *Hydrol. Earth Syst. Sci.*, 24, 3951–3966, <https://doi.org/10.5194/hess-24-3951-2020>, 2020.  
690 Buchanan, B., Auerbach, D. A., Knighton, J., Evensen, D., Fuka, D. R., Easton, Z., Wieczorek, M., Archibald, J. A.,  
691 McWilliams, B., and Walter, T.: Estimating dominant runoff modes across the conterminous United States, *Hydrol. Process.*,  
692 32, 3881–3890, <https://doi.org/10.1002/hyp.13296>, 2018.  
693 Bulygina, N., McIntyre, N., and Wheater, H.: Conditioning rainfall-runoff model parameters for ungauged catchments and  
694 land management impacts analysis, *Hydrol. Earth Syst. Sci.*, 13, 893–904, <https://doi.org/10.5194/hess-13-893-2009>, 2009.  
695 Case, J. L., Mocko, D. M., Hain, C. R., Maina, F. Z., Whitney, K. M., Kumar, S. V., Wade, R. A., Locke, K. A., and White,  
696 K. D.: NLDAS-3: Next-Generation Land Data Assimilation System to Support North American Water-Informed Decisions,  
697 in: 2025 National Soil Moisture Workshop, 2025.  
698 Clark, M., Rupp, D., Woods, R., Meerveld, H., Peters, N., and Freer, J.: Consistency between hydrological models and field  
699 observations: linking processes at the hillslope scale to hydrological responses at the watershed scale, *Hydrological Processes*,  
700 23, 311–319, <https://doi.org/10.1002/HYP.7154>, 2009.



702 Clark, M., Nijssen, B., Lundquist, J., Kavetski, D., Rupp, D., Woods, R., Freer, J., Gutmann, E., Wood, A., Brekke, L., Arnold,  
703 J., Gochis, D., and Rasmussen, R.: A unified approach for process-based hydrologic modeling: 1. Modeling concept, *Water  
704 Resources Research*, 51, 2498–2514, <https://doi.org/10.1002/2015WR017198>, 2015.

705 Clerc-Schwarzenbach, F., Selleri, G., Neri, M., Toth, E., van Meerveld, I., and Seibert, J.: Large-sample hydrology – a few  
706 camels or a whole caravan?, *Hydrol. Earth Syst. Sci.*, 28, 4219–4237, <https://doi.org/10.5194/hess-28-4219-2024>, 2024.

707 Cosgrove, B., Gochis, D., Flowers, T., Dugger, A., Ogden, F., Graziano, T., Clark, E., Cabell, R., Casiday, N., Cui, Z., Eicher,  
708 K., Fall, G., Feng, X., Fitzgerald, K., Frazier, N., George, C., Gibbs, R., Hernandez, L., Johnson, D., Jones, R., Karsten, L.,  
709 Kefelegn, H., Kitzmiller, D., Lee, H., Liu, Y., Mashriqui, H., Mattern, D., McCluskey, A., McCreight, J. L., McDaniel, R.,  
710 Midekisa, A., Newman, A., Pan, L., Pham, C., RafieeiNasab, A., Rasmussen, R., Read, L., Rezaeianzadeh, M., Salas, F., Sang,  
711 D., Sampson, K., Schneider, T., Shi, Q., Sood, G., Wood, A., Wu, W., Yates, D., Yu, W., and Zhang, Y.: NOAA’s National  
712 Water Model: Advancing operational hydrology through continental-scale modeling, *J. Am. Water Resour. Assoc.*, 60, 247–  
713 272, <https://doi.org/10.1111/1752-1688.13184>, 2024.

714 Davis, C. A., Ward, A. S., Burgin, A. J., Loecke, T. D., Riveros-Iregui, D. A., Schnoebelen, D. J., Just, C. L., Thomas, S. A.,  
715 Weber, L. J., and St. Clair, M. A.: Antecedent Moisture Controls on Stream Nitrate Flux in an Agricultural Watershed, *Journal  
716 of Environmental Quality*, 43, 1494–1503, <https://doi.org/10.2134/jeq2013.11.0438>, 2014.

717 DeCicco, L. A., Hirsch, R. M., Lorenz, D., Watkins, D., and Michael Johnson, J.: dataRetrieval, U.S. Geological Survey,  
718 <https://doi.org/10.5066/P9X4L3GE>, 2018.

719 Destouni, G. and Zarei, M.: Water and climate interplay on land in comparative datasets: Revealing unrealistic major drying  
720 bias of climate reanalysis over Africa and the world, AGU FM, 2024, H54B–05, 2024.

721 Dettinger, M. D. and Diaz, H. F.: Global characteristics of stream flow seasonality and variability, *J. Hydrometeorol.*, 1, 289–  
722 310, [https://doi.org/10.1175/1525-7541\(2000\)001<0289:gcosfs>2.0.co;2](https://doi.org/10.1175/1525-7541(2000)001<0289:gcosfs>2.0.co;2), 2000.

723 Dhungel, S., Tarboton, D. G., Jin, J., and Hawkins, C. P.: Potential effects of climate change on ecologically relevant  
724 streamflow regimes: Climate change and streamflow regimes, *River Res. Appl.*, 32, 1827–1840,  
725 <https://doi.org/10.1002/rra.3029>, 2016.

726 Eng, K. and Wolock, D. M.: Evaluation of machine learning approaches for predicting streamflow metrics across the  
727 conterminous United States, 2022–5058, 2022.

728 Estrany, J., Garcia, C., and Batalla, R. J.: Hydrological response of a small mediterranean agricultural catchment, *J. Hydrol.  
729 (Amst.)*, 380, 180–190, <https://doi.org/10.1016/j.jhydrol.2009.10.035>, 2010.

730 Falcone, J.: GAGES-II: Geospatial Attributes of Gages for Evaluating Streamflow, <https://doi.org/10.5066/P96CPHOT>, 2011.

731 Falcone, J. A., Carlisle, D. M., Wolock, D. M., and Meador, M. R.: GAGES: A stream gage database for evaluating natural  
732 and altered flow conditions in the conterminous United States, *Ecology*, 91, 621–621, <https://doi.org/10.1890/09-0889.1>, 2010.

733 Fang, K. and Shen, C.: Full-flow-regime storage-streamflow correlation patterns provide insights into hydrologic functioning  
734 over the continental US, *Water Resour. Res.*, 53, 8064–8083, <https://doi.org/10.1002/2016wr020283>, 2017.



735 Fan, Y., Clark, M., Lawrence, D. M., Swenson, S., Band, L. E., Brantley, S. L., Brooks, P. D., Dietrich, W. E., Flores, A.,  
736 Grant, G., Kirchner, J. W., Mackay, D. S., McDonnell, J. J., Milly, P. C. D., Sullivan, P. L., Tague, C., Ajami, H., Chaney, N.,  
737 Hartmann, A., Hazenberg, P., McNamara, J., Pelletier, J., Perket, J., Rouholahnejad-Freund, E., Wagener, T., Zeng, X.,  
738 Beighley, E., Buzan, J., Huang, M., Livneh, B., Mohanty, B. P., Nijssen, B., Safeeq, M., Shen, C., Verseveld, W., Volk, J.,  
739 and Yamazaki, D.: Hillslope hydrology in global change research and Earth system modeling, *Water Resour. Res.*, 55, 1737–  
740 1772, <https://doi.org/10.1029/2018wr023903>, 2019.

741 Fenicia, F. and McDonnell, J. J.: Modeling streamflow variability regional scale:(1) perceptual model development through  
742 signature analysis, *Journal Hydrology*, 2022.

743 Frame, J. M., Araki, R., Bhuiyan, S. A., Bindas, T., Rapp, J., Bolotin, L., Deardorff, E., Liu, Q., Haces-Garcia, F., Liao, M.,  
744 Frazier, N., and Ogden, F. L.: Machine learning for a heterogeneous water modeling framework, *J. Am. Water Resour. Assoc.*,  
745 61, <https://doi.org/10.1111/1752-1688.70000>, 2025.

746 Gesch, D. B., Evans, G. A., Oimoen, M. J., and Arundel, S.: The National Elevation Dataset: USGS Earth Resources  
747 Observation and Science Center, 2018.

748 Gnann, S., Baldwin, J. W., Cuthbert, M. O., Gleeson, T., Schwanghart, W., and Wagener, T.: The influence of topography on  
749 the global terrestrial water cycle, *Rev. Geophys.*, 63, e2023RG000810, <https://doi.org/10.1029/2023rg000810>, 2025.

750 Gnann, S. J., Howden, N. J. K., and Woods, R. A.: Hydrological signatures describing the translation of climate seasonality  
751 into streamflow seasonality, *Hydrol. Earth Syst. Sci. Discuss.*, 24, 561–580, <https://doi.org/10.5194/hess-24-561-2020>, 2020.

752 Gnann, S. J., McMillan, H. K., Woods, R. A., and Howden, N. J. K.: Including Regional Knowledge Improves Baseflow  
753 Signature Predictions in Large Sample Hydrology, *Water Resour. Res.*, 57, e2020WR028354,  
754 <https://doi.org/10.1029/2020WR028354>, 2021a.

755 Gnann, S. J., Coxon, G., Woods, R. A., Howden, N. J. K., and McMillan, H. K.: TOSSH: A Toolbox for Streamflow Signatures  
756 in Hydrology, *Environmental Modelling & Software*, 138, 104983, <https://doi.org/10.1016/j.envsoft.2021.104983>, 2021b.

757 Golden, H. E., Christensen, J. R., McMillan, H. K., Kelleher, C. A., Lane, C. R., Husic, A., Li, L., Ward, A. S., Hammond, J.,  
758 Seybold, E. C., Jaeger, K. L., Zimmer, M., Sando, R., Jones, C. N., Segura, C., Mahoney, D. T., Price, A. N., and Cheng, F.:  
759 Advancing the science of headwater streamflow for global water protection, *Nat Water*, 1–11, <https://doi.org/10.1038/s44221-024-00351-1>, 2025.

760 Goodrich, D. C., Lane, L. J., Shillito, R. M., Miller, S. N., Syed, K. H., and Woolhiser, D. A.: Linearity of basin response as a  
761 function of scale in a semiarid watershed, *Water Resour. Res.*, 33, 2951–2965, <https://doi.org/10.1029/97wr01422>, 1997.

762 Haines, A., Finlayson, B., and McMahon, T.: A global classification of river regimes, *Applied Geography*, 8, 255–272,  
763 [https://doi.org/10.1016/0143-6228\(88\)90035-5](https://doi.org/10.1016/0143-6228(88)90035-5), 1988.

764 Hammond, J. C.: Daily time series of surface water input from rainfall, rain on snow, and snowmelt for the Conterminous  
765 United States from 1990 to 2023, as well as annual series of input seasonality, precipitation seasonality, and average rainfall,  
766 rain on snow, and snowmelt rates, <https://doi.org/10.5066/P9JWJPNC>, 2024.



768 Hammond, J. C. and Kampf, S. K.: Subannual streamflow responses to rainfall and snowmelt inputs in snow-dominated  
769 watersheds of the western United States, *Water Resour. Res.*, 56, <https://doi.org/10.1029/2019wr026132>, 2020.

770 Hammond, J. C., Zimmer, M., Shanafield, M., Kaiser, K., Godsey, S. E., Mims, M. C., Zipper, S. C., Burrows, R. M., Kampf,  
771 S. K., Dodds, W., Jones, C. N., Krabbenhoft, C. A., Boersma, K. S., Datry, T., Olden, J. D., Allen, G. H., Price, A. N., Costigan,  
772 K., Hale, R., Ward, A. S., and Allen, D. C.: Spatial patterns and drivers of nonperennial flow regimes in the contiguous United  
773 States, *Geophys. Res. Lett.*, 48, <https://doi.org/10.1029/2020gl090794>, 2021.

774 Hammond, J. C., Sextone, G. A., Putman, A. L., Barnhart, T. B., Rey, D. M., Driscoll, J. M., Liston, G. E., Rasmussen, K. L.,  
775 McGrath, D., Fassnacht, S. R., and Kampf, S. K.: High resolution SnowModel simulations reveal future elevation-dependent  
776 snow loss and earlier, flashier surface water input for the upper Colorado river basin, *Earth's Future*, 11,  
777 <https://doi.org/10.1029/2022ef003092>, 2023.

778 Hay, L. E., LaFontaine, J. H., Van Beusekom, A. E., Norton, P. A., Farmer, W. H., Regan, R. S., Markstrom, S. L., and  
779 Dickinson, J. E.: Parameter estimation at the conterminous United States scale and streamflow routing enhancements for the  
780 National Hydrologic Model infrastructure application of the Precipitation-Runoff Modeling System (NHM-PRMS),  
781 <https://doi.org/10.3133/tm6b10>, 2023.

782 Hodgkins, G. A., Renard, B., Whitfield, P. H., Laaha, G., Stahl, K., Hannaford, J., Burn, D. H., Westra, S., Fleig, A. K., Araújo  
783 Lopes, W. T., Murphy, C., Mediero, L., and Hanel, M.: Climate driven trends in historical extreme low streamflows on four  
784 continents, *Water Resour. Res.*, 60, <https://doi.org/10.1029/2022wr034326>, 2024.

785 Holt, A.: New Predictors for Hydrologic Signatures: Wetlands and Geologic Age Across Continental Scales, San Diego State  
786 University, United States -- California, 2024.

787 Holt, A. and McMillan, H.: New predictors for hydrologic signatures: Wetlands and geologic age across continental scales,  
788 *Hydrol. Process.*, 39, <https://doi.org/10.1002/hyp.70080>, 2025.

789 Horton, J. D., San Juan, C. A., and Stoeser, D. B.: The State Geologic Map Compilation (SGMC) geodatabase of the  
790 conterminous United States, <https://doi.org/10.3133/ds1052>, 2017.

791 Hrachowitz, M., Fovet, O., Ruiz, L., Euser, T., Gharari, S., Nijzink, R., Freer, J., Savenije, H. H. G., and Gascuel-Odoux, C.:  
792 Process consistency in models: The importance of system signatures, expert knowledge, and process complexity, *Water Resour.  
793 Res.*, 50, 7445–7469, <https://doi.org/10.1002/2014wr015484>, 2014.

794 Hupp, C. R.: Hydrology, geomorphology and vegetation of Coastal Plain rivers in the south-eastern USA. *Hydrological  
795 processes*, 14, 2991–3010, 2000.

796 Husic, A.: Game theory for catchment science, *ESS Open Archive*, <https://doi.org/10.22541/essoar.173924202.27840286/v1>,  
797 2025.

798 Husic, A., Hammond, J., Price, A. N., and Roundy, J. K.: Interrogating process deficiencies in large-scale hydrologic models  
799 with interpretable machine learning, *Hydrol. Earth Syst. Sci.*, 29, 4457–4472, <https://doi.org/10.5194/hess-29-4457-2025>,  
800 2025.



801 Jackisch, C., Angermann, L., Allroggen, N., Sprenger, M., Blume, T., Tronicke, J., and Zehe, E.: Form and function in hillslope  
802 hydrology: in situ imaging and characterization of flow-relevant structures, *Hydrol. Earth Syst. Sci.*, 21, 3749–3775, 2017.

803 Janssen, J. and Ameli, A. A.: A hydrologic functional approach for improving large-sample hydrology performance in poorly  
804 gauged regions, *Water Resour. Res.*, 57, <https://doi.org/10.1029/2021wr030263>, 2021.

805 Jefferson, A., Grant, G. E., Lewis, S. L., and Lancaster, S. T.: Coevolution of hydrology and topography on a basalt landscape  
806 in the Oregon Cascade Range, USA, *Earth Surf. Process.*, <https://doi.org/10.1002/esp.1976>, 2010.

807 Ji, H., Song, Y., Bindas, T., Shen, C., Yang, Y., Pan, M., Liu, J., Rahmani, F., Abbas, A., Beck, H., Lawson, K., and Wada,  
808 Y.: Distinct hydrologic response patterns and trends worldwide revealed by physics-embedded learning, *arXiv [physics.geo-  
809 ph]*, *arXiv*, 2025.

810 Johnson, J. M., Fang, S., Sankarasubramanian, A., Rad, A. M., Kindl da Cunha, L., Jennings, K. S., Clarke, K. C., Mazrooei,  
811 A., and Yeghiazarian, L.: Comprehensive analysis of the NOAA National Water Model: A call for heterogeneous formulations  
812 and diagnostic model selection, *J. Geophys. Res.*, 128, <https://doi.org/10.1029/2023jd038534>, 2023.

813 Kavetski, D. and Fenicia, F.: Elements of a flexible approach for conceptual hydrological modeling: 2. Application and  
814 experimental insights, *Water Resour. Res.*, 47, <https://doi.org/10.1029/2011wr010748>, 2011.

815 Kennard, M. J., Pusey, B. J., Olden, J. D., Mackay, S. J., Stein, J. L., and Marsh, N.: Classification of natural flow regimes in  
816 Australia to support environmental flow management: Classification of natural flow regimes in Australia, *Freshw. Biol.*, 55,  
817 171–193, <https://doi.org/10.1111/j.1365-2427.2009.02307.x>, 2010.

818 Kiang, J. E., Stewart, D. W., Archfield, S. A., Osborne, E. B., and Eng, K.: A national streamflow network gap analysis (No.  
819 2013-5013), US Geological Survey, 2013.

820 Knoben, W. J. M., Woods, R. A., and Freer, J. E.: A quantitative hydrological climate classification evaluated with independent  
821 streamflow data, *Water Resour. Res.*, 54, 5088–5109, <https://doi.org/10.1029/2018wr022913>, 2018.

822 Knoben, W. J. M., Freer, J. E., Peel, M. C., Fowler, K. J. A., and Woods, R. A.: A brief analysis of conceptual model structure  
823 uncertainty using 36 models and 559 catchments, *Water Resour. Res.*, 56, e2019WR025975,  
824 <https://doi.org/10.1029/2019wr025975>, 2020.

825 Krabbenhoft, C. A., Allen, G. H., Lin, P., Godsey, S. E., Allen, D. C., Burrows, R. M., DelVecchia, A. G., Fritz, K. M.,  
826 Shanafield, M., Burgin, A. J., Zimmer, M. A., Datry, T., Dodds, W. K., Jones, C. N., Mims, M. C., Franklin, C., Hammond, J.  
827 C., Zipper, S., Ward, A. S., Costigan, K. H., Beck, H. E., and Olden, J. D.: Assessing placement bias of the global river gauge  
828 network, *Nat. Sustain.*, 5, 586–592, <https://doi.org/10.1038/s41893-022-00873-0>, 2022.

829 Kratzert, F., Nearing, G., Addor, N., Erickson, T., Gauch, M., Gilon, O., Gudmundsson, L., Hassidim, A., Klotz, D., Nevo, S.,  
830 Shalev, G., and Matias, Y.: Caravan - A global community dataset for large-sample hydrology, *Sci Data*, 10, 61,  
831 <https://doi.org/10.1038/s41597-023-01975-w>, 2023.

832 Kratzert, F., Nearing, G., Addor, N., Erickson, T., Gauch, M., Gilon, O., Gudmundsson, L., Hassidim, A., Klotz, D., Nevo, S.,  
833 Shalev, G., and Matias, Y.: Caravan - A global community dataset for large-sample hydrology Version 1.4,  
834 <https://doi.org/10.5281/ZENODO.10968468>, 2024.



835 Kuentz, A., Arheimer, B., Hundecha, Y., and Wagener, T.: Understanding hydrologic variability across Europe through  
836 catchment classification, *Hydrol. Earth Syst. Sci.*, 21, 2863–2879, 2017.

837 Kuhn, M.: Building predictive models in R using the caret package, *Journal of Statistical Software*, 28, 1–26,  
838 <https://doi.org/10.18637/JSS.V028.I05>, 2008.

839 Lane, B. A., Dahlke, H. E., Pasternack, G. B., and Sandoval-Solis, S.: Revealing the Diversity of Natural Hydrologic Regimes  
840 in California with Relevance for Environmental Flows Applications, *J. Am. Water Resour. Assoc.*, 53, 411–430,  
841 <https://doi.org/10.1111/1752-1688.12504>, 2017.

842 Lane, C. R. and D'Amico, E.: Identification of putative geographically isolated wetlands of the conterminous United States, *J.*  
843 *Am. Water Resour. Assoc.*, 52, 705–722, <https://doi.org/10.1111/1752-1688.12421>, 2016.

844 Lapides, D. A., Zipper, S., and Hammond, J. C.: Identifying hydrologic signatures associated with streamflow depletion caused  
845 by groundwater pumping, *Hydrol. Process.*, 37, <https://doi.org/10.1002/hyp.14877>, 2023.

846 Lee, D., Ward, P., and Block, P.: Defining high-flow seasons using temporal streamflow patterns from a global model, *Hydrol.*  
847 *Earth Syst. Sci.*, 19, 4689–4705, <https://doi.org/10.5194/hess-19-4689-2015>, 2015.

848 Linke, S., Lehner, B., Ouellet Dallaire, C., Ariwi, J., Grill, G., Anand, M., Beames, P., Burchard-Levine, V., Maxwell, S.,  
849 Moidu, H., Tan, F., and Thieme, M.: Global hydro-environmental sub-basin and river reach characteristics at high spatial  
850 resolution, *Sci Data*, 6, 283, <https://doi.org/10.1038/s41597-019-0300-6>, 2019.

851 Lins, H. F.: Regional streamflow regimes and hydroclimatology of the United States, *Water Resour. Res.*, 33, 1655–1667,  
852 <https://doi.org/10.1029/97WR00615>, 1997.

853 Lohse, K. A. and Dietrich, W. E.: Contrasting effects of soil development on hydrological properties and flow paths, *Water*  
854 *Resour. Res.*, 41, <https://doi.org/10.1029/2004wr003403>, 2005.

855 Lundberg, S. and Lee, S.-I.: A unified approach to interpreting model predictions, *arXiv [cs.AI]*, arXiv, 2017.

856 Lundberg, S. M., Erion, G. G., and Lee, S.-I.: Consistent individualized feature attribution for tree ensembles, *arXiv [cs.LG]*,  
857 arXiv, 2018.

858 Markstrom, S. L., Hay, L. E., and Clark, M. P.: Towards simplification of hydrologic modeling: identification of dominant  
859 processes, *Hydrol. Earth Syst. Sci.*, 20, 4655–4671, <https://doi.org/10.5194/hess-20-4655-2016>, 2016.

860 Mazvimavi, D., Meijerink, A. M. J., Savenije, H. H. G., and Stein, A.: Prediction of flow characteristics using multiple  
861 regression and neural networks: A case study in Zimbabwe, *Phys. Chem. Earth* (2002), 30, 639–647,  
862 <https://doi.org/10.1016/j.pce.2005.08.003>, 2005.

863 McGrath, G. S., Hinz, C., and Sivapalan, M.: Temporal dynamics of hydrological threshold events, *Hydrol. Earth Syst. Sci.*,  
864 11, 923–938, <https://doi.org/10.5194/hess-11-923-2007>, 2007.

865 McMillan, H.: Linking hydrologic signatures to hydrologic processes: A Review, *Hydrol. Process.*, 34, 1393–1409,  
866 <https://doi.org/10.1002/hyp.13632>, 2020.



867 McMillan, H., Gueguen, M., Grimon, E., Woods, R., Clark, M., and Rupp, D. E.: Spatial variability of hydrological processes  
868 and model structure diagnostics in a 50 km<sup>2</sup> catchment, *Hydrol. Process.*, 28, 4896–4913, <https://doi.org/10.1002/hyp.9988>,  
869 2014.

870 McMillan, H., Westerberg, I., and Branger, F.: Five guidelines for selecting hydrological signatures, *Hydrol. Process.*, 31,  
871 4757–4761, <https://doi.org/10.1002/hyp.11300>, 2017.

872 McMillan, H., Araki, R., Bolotin, L., Kim, D.-H., Coxon, G., Clark, M., and Seibert, J.: Global patterns in observed hydrologic  
873 processes, *Nat Water*, <https://doi.org/10.1038/s44221-025-00407-w>, 2025.

874 McMillan, H. K.: A review of hydrologic signatures and their applications, *WIREs Water*, 8, <https://doi.org/10.1002/wat2.1499>,  
875 2021.

876 McMillan, H. K., Gnann, S. J., and Araki, R.: Large scale evaluation of relationships between hydrologic signatures and  
877 processes, *Water Resour. Res.*, 58, <https://doi.org/10.1029/2021wr031751>, 2022.

878 McMillan, H. K., Coxon, G., Araki, R., Salwey, S., Kelleher, C., Zheng, Y., Knoben, W., Gnann, S., Seibert, J., and Bolotin,  
879 L.: When good signatures go bad: Applying hydrologic signatures in large sample studies, *Hydrol. Process.*, 37,  
880 <https://doi.org/10.1002/hyp.14987>, 2023.

881 Miller, D. A. and White, R. A.: A conterminous United States multilayer soil characteristics dataset for regional climate and  
882 hydrology modeling, *Earth Interact.*, 2, 1–26, [https://doi.org/10.1175/1087-3562\(1998\)002<0001:acusms>2.3.co;2](https://doi.org/10.1175/1087-3562(1998)002<0001:acusms>2.3.co;2), 1998.

883 Miller, J. A.: Ground water atlas of the United States: Introduction and national summary (No. 730-A), A1–A15, 1999.

884 Molnar, C., Bischl, B., and Casalicchio, G.: iml: An R package for Interpretable Machine Learning,  
885 <https://doi.org/10.21105/joss.00786>, 2018.

886 Mosley, M. P.: Delimitation of New Zealand hydrologic regions, *J. Hydrol. (Amst.)*, 49, 173–192,  
887 [https://doi.org/10.1016/0022-1694\(81\)90211-0](https://doi.org/10.1016/0022-1694(81)90211-0), 1981.

888 Muñoz Sabater, J.: ERA5-Land monthly averaged data from 1950 to present, <https://doi.org/10.24381/CDS.68D2BB30>, 2019.

889 Neff, B. P., Day, S. M., Piggott, A. R., and Fuller, L. M.: Base flow in the Great Lakes Basin,  
890 <https://doi.org/10.3133/sir20055217>, 2005.

891 Noguchi, S., Nik, A. R., Yusop, Z., Tani, M., and Sammori, T.: Rainfall-runoff responses and roles of soil moisture variations  
892 to the response in tropical Rain Forest, Bukit Tarek, peninsular Malaysia, *J. Forest Res.*, 2, 125–132,  
893 <https://doi.org/10.1007/bf02348209>, 1997.

894 Ogden, F., Avant, B., Bartel, R., Blodgett, D., Clark, E., Coon, E., Cosgrove, B., Cui, S., Kindl da Cunha, L., Farthing, M.,  
895 Flowers, T., Frame, J., Frazier, N., Graziano, T., Gutenson, J., Johnson, D., McDaniel, R., Moulton, J., Loney, D., Peckham,  
896 S., Mattern, D., Jennings, K., Williamson, M., Savant, G., Tubbs, C., Garrett, J., Wood, A., and Johnson, J.: The Next  
897 Generation Water Resources Modeling Framework: Open Source, Standards Based, Community Accessible, Model  
898 Interoperability for Large Scale Water Prediction, *AGU Fall Meeting Abstracts*, New Orleans, LA, 2021, H43D–01, 2021.

899 Omernik, J. M.: Ecoregions of the conterminous United States, *Ann. Assoc. Am. Geogr.*, 77, 118–125, 1987.



900 Omernik, J. M.: Perspectives on the nature and definition of ecological regions, *Environ. Manage.*, 34 Suppl 1, S27–38,  
901 <https://doi.org/10.1007/s00267-003-5197-2>, 2004.

902 Oswald, C. J., Kelleher, C., Ledford, S. H., Hopkins, K. G., Sytsma, A., Tetzlaff, D., Toran, L., and Voter, C.: Integrating  
903 urban water fluxes and moving beyond impervious surface cover: A review, *J. Hydrol. (Amst.)*, 618, 129188,  
904 <https://doi.org/10.1016/j.jhydrol.2023.129188>, 2023.

905 Oudin, L., Andréassian, V., Perrin, C., Michel, C., and Le Moine, N.: Spatial proximity, physical similarity, regression and  
906 ungaged catchments: A comparison of regionalization approaches based on 913 French catchments, *Water Resources Research*,  
907 44, <https://doi.org/10.1029/2007WR006240>, 2008.

908 Paola, C., Foufoula-Georgiou, E., Dietrich, W. E., Hondzo, M., Mohrig, D., Parker, G., Power, M. E., Rodriguez-Iturbe, I.,  
909 Voller, V., and Wilcock, P.: Toward a unified science of the Earth's surface: Opportunities for synthesis among hydrology,  
910 geomorphology, geochemistry, and ecology, *Water Resour. Res.*, 42, <https://doi.org/10.1029/2005wr004336>, 2006.

911 Pechlivanidis, I. G. and Arheimer, B.: Large-scale hydrological modelling by using modified PUB recommendations: the  
912 India-HYPE case, *Hydrol. Earth Syst. Sci.*, 19, 4559–4579, <https://doi.org/10.5194/hess-19-4559-2015>, 2015.

913 Pedregosa, F., Varoquaux, G., Gramfort, A., Michel, V., Thirion, B., Grisel, O., Blondel, M., Prettenhofer, P., Weiss, R.,  
914 Dubourg, V., Vanderplas, J., Passos, A., Cournapeau, D., Brucher, M., Perrot, M., and Duchesnay, E.: Scikit-learn: Machine  
915 Learning in Python, *Journal of Machine Learning Research*, 12, 2825–2830, 2011.

916 Penna, D.: A recipe for why and how to set up and sustain an experimental catchment, *Hydrol. Process.*, 38,  
917 <https://doi.org/10.1002/hyp.15163>, 2024.

918 Peters, N. E. and Aulenbach, B. T.: Water storage at the Panola mountain research watershed, Georgia, USA: Water storage  
919 at pmrw, *Hydrol. Process.*, 25, 3878–3889, <https://doi.org/10.1002/hyp.8334>, 2011.

920 Pfister, L., Martínez-Carreras, N., Hissler, C., Klaus, J., Carrer, G. E., Stewart, M. K., and McDonnell, J. J.: Bedrock geology  
921 controls on catchment storage, mixing, and release: A comparative analysis of 16 nested catchments, *Hydrological Processes*,  
922 31, 1828–1845, <https://doi.org/10.1002/hyp.11134>, 2017.

923 Prieto, C., Kavetski, D., Le Vine, N., Álvarez, C., and Medina, R.: Identification of dominant hydrological mechanisms using  
924 Bayesian inference, multiple statistical hypothesis testing, and flexible models, *Water Resour. Res.*, 57,  
925 <https://doi.org/10.1029/2020wr028338>, 2021.

926 Qi, S. L. and Mason, C. A.: Data used to prioritize the selection of river basins for intensive monitoring and assessment by the  
927 U.S. Geological Survey, <https://doi.org/10.5066/P98194QR>, 2023.

928 R Core Team (2024). R: A Language and Environment for Statistical Computing. R Foundation for Statistical Computing,  
929 Vienna, Austria. <https://www.R-project.org/>.

930 Reinecke, R., Stein, L., Gnann, S., Andersson, J. C. M., Arheimer, B., Bierkens, M., Bonetti, S., Güntner, Kollet, S., Mishra,  
931 S., Moosdorf, N., Nazari, S., Pokhrel, Y., Prudhomme, C., Schewe, J., Shen, C., and Wagener, T.: Uncertainties guide global  
932 water model advancement, *WIREs Water*, 12, <https://doi.org/10.1002/wat2.70025>, 2025.



933 Robert Maier, H., Rosa Taghikhah, F., Nabavi, E., Razavi, S., Gupta, H., Wu, W., Radford, D. A. G., and Huang, J.: How  
934 much X is in XAI: Responsible use of “Explainable” artificial intelligence in hydrology and water resources, *J. Hydrol.* X, 25,  
935 100185, <https://doi.org/10.1016/j.hydroa.2024.100185>, 2024.

936 Safeeq, M. and Hunsaker, C. T.: Characterizing runoff and water yield for headwater catchments in the southern Sierra Nevada,  
937 *J. Am. Water Resour. Assoc.*, 52, 1327–1346, <https://doi.org/10.1111/1752-1688.12457>, 2016.

938 Safeeq, M., Grant, G. E., Lewis, S. L., and Tague, C. L.: Coupling snowpack and groundwater dynamics to interpret historical  
939 streamflow trends in the western United States: COUPLING SNOWPACK AND GROUNDWATER DYNAMICS TO  
940 INTERPRET STREAMFLOW, *Hydrol. Process.*, 27, 655–668, <https://doi.org/10.1002/hyp.9628>, 2013.

941 Santhi, C., Allen, P. M., Muttiah, R. S., Arnold, J. G., and Tuppad, P.: Regional estimation of base flow for the conterminous  
942 United States by hydrologic landscape regions, *J. Hydrol. (Amst.)*, 351, 139–153,  
943 <https://doi.org/10.1016/j.jhydrol.2007.12.018>, 2008.

944 Sauquet, E., Shanafield, M., Hammond, J. C., Sefton, C., Leigh, C., and Datry, T.: Classification and trends in intermittent  
945 river flow regimes in Australia, northwestern Europe and USA: A global perspective, *J. Hydrol. (Amst.)*, 597, 126170,  
946 <https://doi.org/10.1016/j.jhydrol.2021.126170>, 2021.

947 Seaber, P. R., Kapinos, F. P., and Knapp, G. L.: Hydrologic unit maps, US Geological Survey, <https://doi.org/10.3133/wsp2294>,  
948 1987.

949 Sebestyen, S. D., Shanley, J. B., Blume, T., Duncan, J. M., Jones, J., Segura, C., and Mast, M. A.: Introduction to the special  
950 issue on research and observatory catchments, *Hydrol. Process.*, 39, <https://doi.org/10.1002/hyp.70069>, 2025.

951 Shalev, G. and Kratzert, F.: Caravan MultiMet: Extending Caravan with multiple weather nowcasts and forecasts, *arXiv*  
952 [cs.LG], *arXiv*, 2024.

953 Shapley, L. S.: 17. A Value for n-Person Games, in: *Contributions to the Theory of Games (AM-28)*, Volume II, edited by:  
954 Kuhn, H. W. and Tucker, A. W., Princeton University Press, Princeton, 307–318, <https://doi.org/10.1515/9781400881970-018>,  
955 1953.

956 Shaw, S. B. and Riha, S. J.: Examining individual recession events instead of a data cloud: Using a modified interpretation of  
957  $dQ/dt - Q$  streamflow recession in glaciated watersheds to better inform models of low flow, *J. Hydrol. (Amst.)*, 434–435, 46–  
958 54, <https://doi.org/10.1016/j.jhydrol.2012.02.034>, 2012.

959 Shrestha, D., Howard, D., and Benedict, T. D.: Moderate Resolution Imaging Spectroradiometer (MODIS) irrigated  
960 Agriculture datasets for the conterminous United States (MIRAD-US), <https://doi.org/10.5066/P9NA3EO8>, 2019.

961 Sivapalan, M.: Pattern, process and function: Elements of a unified theory of hydrology at the catchment scale, in:  
962 *Encyclopedia of Hydrological Sciences*, Wiley, Chichester, UK, <https://doi.org/10.1002/0470848944.hsa012>, 2005.

963 Web Soil Survey: <http://websoilsurvey.nrcs.usda.gov/>, last access: 11 May 2025.

964 Spieler, D., Mai, J., Craig, J. R., Tolson, B. A., and Schütze, N.: Automatic model structure identification for conceptual  
965 hydrologic models, *Water Resour. Res.*, 56, <https://doi.org/10.1029/2019wr027009>, 2020.



966 Stets, E. G., Archer, A. A., Degnan, J. R., Erickson, M. L., Gorski, G., Medalie, L., and Scholl, M. A.: The National integrated  
967 water availability assessment, 2025.

968 Tague, C. and Grant, G. E.: A geological framework for interpreting the low-flow regimes of Cascade streams, Willamette  
969 River Basin, Oregon: GEOLOGICAL FRAMEWORK FOR LOW-FLOW REGIMES, Water Resour. Res., 40,  
970 <https://doi.org/10.1029/2003wr002629>, 2004.

971 Tague, C. and Grant, G. E.: Groundwater dynamics mediate low-flow response to climate warming in snow-dominated alpine  
972 regions, Water Resources Research, 45, 2009.

973 Tallaksen, L. M.: A review of baseflow recession analysis, J. Hydrol., 165, 349–370, [https://doi.org/10.1016/0022-1694\(94\)02540-R](https://doi.org/10.1016/0022-1694(94)02540-R), 1995.

975 Tarasova, L., Gnann, S., Yang, S., Hartmann, A., and Wagener, T.: Catchment characterization: Current descriptors,  
976 knowledge gaps and future opportunities, Earth Sci. Rev., 252, 104739, <https://doi.org/10.1016/j.earscirev.2024.104739>, 2023.

977 Thompson, J. M., Hathaway, J. M., Perfect, E., and Schwartz, J. S.: The effect of stormwater infiltration and surrounding built  
978 infrastructure on local groundwater dynamics: a case study for regenerative stormwater conveyances, Sustain. Resilient  
979 Infrastruct., 1–11, <https://doi.org/10.1080/23789689.2020.1772636>, 2020.

980 Trancoso, R., Phinn, S., McVicar, T., Larsen, J., and McAlpine, C.: Regional variation in streamflow drivers across a  
981 continental climatic gradient, Ecohydrology, 10, e1816, <https://doi.org/10.1002/eco.1816>, 2017.

982 Tran, V. N.: CAMELSh: A large-sample hourly hydrometeorological dataset and attributes at watershed-scale for contiguous  
983 United States, <https://doi.org/10.5281/ZENODO.15070091>, 2025.

984 Tran, V. N., Xu, D., Van Nguyen, T., Kim, T., and Ivanov, V. Y.: CAMELSh: A large-sample hourly hydrometeorological  
985 dataset and attributes at watershed-scale for CONUS, Sci. Data, 12, 1307, <https://doi.org/10.1038/s41597-025-05612-6>, 2025.

986 Turner, S., Hannaford, J., Barker, L. J., Suman, G., Killeen, A., Armitage, R., Chan, W., Davies, H., Griffin, A., Kumar, A.,  
987 Dixon, H., Albuquerque, M. T. D., Almeida Ribeiro, N., Alvarez-Garreton, C., Amoussou, E., Arheimer, B., Asano, Y.,  
988 Berezowski, T., Bodian, A., Boutaghane, H., Capell, R., Dakhaoui, H., Daňhelka, J., Do, H. X., Ekkawatpanit, C., El Khalki,  
989 E. M., Fleig, A. K., Fonseca, R., Giraldo-Osorio, J. D., Goula, A. B. T., Hanel, M., Horton, S., Kan, C., Kingston, D. G., Laaha,  
990 G., Laugesen, R., Lopes, W., Mager, S., Rachdane, M., Markonis, Y., Medeiro, L., Midgley, G., Murphy, C., O'Connor, P.,  
991 Pedersen, A. I., Pham, H. T., Piniewski, M., Renard, B., Saidi, M. E., Schmocker-Fackel, P., Stahl, K., Thyer, M., Toucher,  
992 M., Tramblay, Y., Uusikivi, J., Venegas-Cordero, N., Visessri, S., Watson, A., Westra, S., and Whitfield, P. H.: ROBIN:  
993 Reference observatory of basins for international hydrological climate change detection, Sci. Data, 12, 654,  
994 <https://doi.org/10.1038/s41597-025-04907-y>, 2025.

995 UKIH: UK Institute of Hydrology (Great Britain), Low Flow Studies Reports, Institute of Hydrology, 1980.

996 United States Department of Agriculture, Soil Survey Staff, and Natural Resources Conservation: U.S. General Soil Map  
997 (STATSGO): Web soil survey, 2008.

998 United States Geological Survey: Protected Areas Database of the United States (PAD-US) 4,  
999 <https://doi.org/10.5066/P96WBCHS>, 2024.



1000 U.S. Environmental Protection Agency: National Hydrography Dataset Plus (NHDPlus): USEPA; USGS; and Horizon  
1001 Systems Corporation, 2008.

1002 U.S. Geological Survey: USGS Water Data for the Nation: U.S. Geological Survey National Water Information System  
1003 Database, <https://doi.org/10.5066/F7P55KJN>, 2025.

1004 Valeron, B. and Meixner, T.: Overland flow generation in chaparral ecosystems: temporal and spatial variability, *Hydrol.*  
1005 *Process.*, 24, 65–75, <https://doi.org/10.1002/hyp.7455>, 2010.

1006 Van Metre, P. C., Qi, S., Deacon, J., Dieter, C., Driscoll, J. M., Fienen, M., Kenney, T., Lambert, P., Lesmes, D., Mason, C.  
1007 A., Mueller-Solger, A., Musgrove, M., Painter, J., Rosenberry, D., Sprague, L., Tesoriero, A. J., Windham-Myers, L., and  
1008 Wolock, D.: Prioritizing river basins for intensive monitoring and assessment by the US Geological Survey, *Environ. Monit.  
1009 Assess.*, 192, 458, <https://doi.org/10.1007/s10661-020-08403-1>, 2020.

1010 Westerberg, I. K., Wagener, T., Coxon, G., McMillan, H. K., Castellarin, A., Montanari, A., and Freer, J.: Uncertainty in  
1011 hydrological signatures for gauged and ungauged catchments, *Water Resources Research*, 52, 1847–1865,  
1012 <https://doi.org/10.1002/2015WR017635>, 2016.

1013 Wieczorek, M. E. and LaMotte, A. E.: Attributes for NHDPlus Catchments (Version 1.1) for the Conterminous United States:  
1014 Average Saturation Excess-Overland Flow, 2002: U.S. Geological Survey data release, 2010.

1015 Wieczorek, M. E., Hafen, K. C., and Staub, L. E.: Data-Driven Drought Prediction Project model inputs for Upper and Lower  
1016 Colorado portions of the national hydrologic Geo-spatial fabric version 1.1 and select U.S. geological Survey streamgage basins  
1017 (ver. 2.0, July 2025), <https://doi.org/10.5066/P98IG8LO>, 2023.

1018 Willard, J. D., Ciulla, F., Weierbach, H., Kumar, V., and Varadharajan, C.: Evaluating deep learning approaches for predictions  
1019 in unmonitored basins with continental-scale stream temperature models, *arXiv [cs.LG]*, arXiv, 2024.

1020 Williams, P. W. and Ford, D. C.: Global distribution of carbonate rocks, *Zeitschrift für Geomorphologie Suppl.*, 147, 1–2, 2006.

1021 Wilson, C. G., Papanicolaou, A. N. T., and Denn, K. D.: Partitioning fine sediment loads in a headwater system with intensive  
1022 agriculture, *J. Soils Sediments*, 12, 966–981, <https://doi.org/10.1007/s11368-012-0504-2>, 2012.

1023 Winter, T. C.: The Concept of Hydrologic Landscapes, *JAWRA Journal of the American Water Resources Association*, 37,  
1024 335–349, <https://doi.org/10.1111/j.1752-1688.2001.tb00973.x>, 2001.

1025 Wlostowski, A. N., Molotch, N., Anderson, S. P., Brantley, S. L., Chorover, J., Dralle, D., Kumar, P., Li, L., Lohse, K. A.,  
1026 Mallard, J. M., McIntosh, J. C., Murphy, S. F., Parrish, E., Safeeq, M., Seyfried, M., Shi, Y., and Harman, C.: Signatures of  
1027 Hydrologic Function Across the Critical Zone Observatory Network, *Water Resour. Res.*, 57, e2019WR026635,  
1028 <https://doi.org/10.1029/2019wr026635>, 2021.

1029 Wolock, D. M.: Hydrologic landscape regions of the United States, US Geological Service, 2003a.

1030 Wolock, D. M.: Infiltration-excess overland flow estimated by TOPMODEL for the conterminous United States (No. 2003-  
1031 310), US Geological Survey., 2003b.

1032 Wu, S., Zhao, J., Wang, H., and Sivapalan, M.: Regional patterns and physical controls of streamflow generation across the  
1033 conterminous United States, *Water Resour. Res.*, 57, e2020WR028086, <https://doi.org/10.1029/2020wr028086>, 2021.



1034 Xia, Y., Mitchell, K., Ek, M., Sheffield, J., Cosgrove, B., Wood, E., Luo, L., Alonge, C., Wei, H., Meng, J., Livneh, B.,  
1035 Lettenmaier, D., Koren, V., Duan, Q., Mo, K., Fan, Y., and Mocko, D.: Continental-scale water and energy flux analysis and  
1036 validation for the North American Land Data Assimilation System project phase 2 (NLDAS-2): 1. Intercomparison and  
1037 application of model products, *J. Geophys. Res. D: Atmos.*, 117, <https://doi.org/10.1029/2011JD016048>, 2012.

1038 Xie, J., Liu, X., Jasechko, S., Berghuijs, W. R., Wang, K., Liu, C., Reichstein, M., Jung, M., and Koirala, S.: Majority of global  
1039 river flow sustained by groundwater, *Nat. Geosci.*, 17, 770–777, <https://doi.org/10.1038/s41561-024-01483-5>, 2024.

1040 Yang, L., Jin, S., Danielson, P., Homer, C., Gass, L., Bender, S. M., Case, A., Costello, C., Dewitz, J., Fry, J., Funk, M.,  
1041 Granneman, B., Liknes, G. C., Rigge, M., and Xian, G.: A new generation of the United States National Land Cover Database:  
1042 Requirements, research priorities, design, and implementation strategies, *ISPRS J. Photogramm. Remote Sens.*, 146, 108–123,  
1043 <https://doi.org/10.1016/j.isprsjprs.2018.09.006>, 2018.

1044 Yilmaz, K. K., Gupta, H. V., and Wagener, T.: A process-based diagnostic approach to model evaluation: Application to the  
1045 NWS distributed hydrologic model, *Water Resour. Res.*, 44, <https://doi.org/10.1029/2007wr006716>, 2008.

1046 Zimmer, M. A. and Gannon, J. P.: Run-off processes from mountains to foothills: The role of soil stratigraphy and structure  
1047 in influencing run-off characteristics across high to low relief landscapes, *Hydrol. Process.*, 32, 1546–1560,  
1048 <https://doi.org/10.1002/hyp.11488>, 2018.

1049 Zipper, S. C., Hammond, J. C., Shanafield, M., Zimmer, M., Datry, T., Jones, C. N., Kaiser, K. E., Godsey, S. E., Burrows, R.  
1050 M., Blaszcak, J. R., Busch, M. H., Price, A. N., Boersma, K. S., Ward, A. S., Costigan, K., Allen, G. H., Krabbenhoft, C. A.,  
1051 Dodds, W. K., Mims, M. C., Olden, J. D., Kampf, S. K., Burgin, A. J., and Allen, D. C.: Pervasive changes in stream  
1052 intermittency across the United States, *Environ. Res. Lett.*, 16, 084033, <https://doi.org/10.1088/1748-9326/ac14ec>, 2021.